Climate Dynamics
https://doi.org/10.1007/s00382-023-06817-4

Modulations in the Indian Summer Monsoon–ENSO teleconnections by the North Tropical Atlantic

K. P. Sooraj[1] · Ajinkya M. Aswale[1,2] · P. Swapna[1] · P. Terray[3] · N. S. Sandeep[1]

Received: 10 November 2022 / Accepted: 1 May 2023

Abstract
North Tropical Atlantic Sea Surface Temperature (i.e., NTA SST) anomalies emerge as a key-driver of the whole El Niño Southern Oscillation–Indian Summer Monsoon (ENSO–ISM) system. However, as the underlying physical mechanisms are not yet well understood, this study made an attempt to have deeper insights on the role of the NTA SST variability on the ISM, ENSO and their mutual relationships. The evidences from observations and a Pi-Control coupled simulation demonstrate the pronounced biennial nature of the NTA–ENSO–ISM system and suggest the precursory role of the NTA SSTs in this biennial ENSO–ISM system. As the cause-and-effect relationships are difficult to disentangle, ensembles of short coupled sensitivity experiments are conducted by imposing observed warm (cold) SST anomalies over NTA. These 1-year simulations start from various January initial conditions corresponding to strong El Niño (La Niña) events as identified from Pi-Control and subsequently impose warm (cold) SST anomalies over the NTA region after the El Niño (La Niña) peak in January. The sensitivity experiments support the hypothesis of a key role of NTA SSTs in the reversal of the ENSO conditions through their capacitor effect. They further illustrate the nonlinear characteristics of this system as cold NTA SST perturbations are more influential than warm NTA SSTs. This non-linearity brings up new perspectives on the NTA–ENSO–ISM system, as it is further reflected in the asymmetric response in the simulated ENSO–ISM, with the cold NTA perturbations initiated from the La Niña conditions showing a stronger anomalous ISM response during boreal summer, which is in contrast with the feeble ISM response in the warm NTA perturbations experiment using the El Niño initial conditions. This non-linearity of NTA–ENSO–ISM has larger implications in a global warming scenario, as the climate variability over NTA region is projected to intensify in the future.

Keywords ISM response · ENSO · NTA SST · NTA–ENSO–ISM association · Asymmetric ENSO–ISM response · Coupled model simulations

1 Introduction

The south Asian summer monsoon (e.g., Indian Summer Monsoon, ISM) during June–September (JJAS) is a major component of the global hydrological cycle providing food and energy security to approximately half of the world's population. India receives over 75% of its annual precipitation during the JJAS period (Parthasarathy et al. 1994). The ISM Rainfall (ISMR) has shown a declining trend since mid-twentieth century (e.g., Masson-Delmotte et al. 2021), but, the recent Intergovernmental Panel on Climate Change Sixth Assessment Report (IPCC AR6) shows that the ISMR is projected to intensify with global warming during the twenty-first century, with enhanced interannual variability (Douville et al. 2021; Katzenberger et al. 2021). Considering the socio-economic relevance of ISMR in sustainable developments, precise understanding of the present-day ISMR variability is of utmost importance, as in the context of a changing climate the knowledge so acquired can be used to ensure food and energy security to the south Asian region (especially India) in the coming decades.

✉ K. P. Sooraj
sooraj@tropmet.res.in

[1] Centre for Climate Change Research, Indian Institute of Tropical Meteorology, Ministry of Earth Sciences, Pune 411008, India

[2] Department of Atmospheric and Space Sciences, Savitribai Phule Pune University, Pune 411007, India

[3] Sorbonne Universites (UPMC, Univ Paris 06)-CNRS-IRD-MNHN, LOCEAN Laboratory, 4 Place Jussieu, Paris, France

Published online: 17 May 2023

As the interannual variability of ISMR is also projected to increase in the coming decades with the coupled models participated in IPCC AR6 exhibiting huge intermodel spread (Katzenberger et al. 2021), the dominant modes of climate variability influencing ISMR need further attention. El Niño Southern Oscillation (ENSO) is one of the dominant drivers of ISMR interannual variability (e.g., Webster et al. 1998). In addition to ENSO, it is generally agreed that many other climatic modes may also modulate the ISMR interannual variability (e.g., Chowdary et al. 2021 and the references therein).

Firstly, the relationship between ISMR and Indian Ocean Sea Surface Temperature (SST) anomalies is highlighted and illustrated (e.g., Indian Ocean Dipole, IOD, Cherchi et al. 2021). However, there are still ongoing debates on the potential role of IOD on ISMR due to the complex association of IOD with the ENSO–ISM system (e.g., Crétat et al. 2017; Terray et al. 2021; Chakraborty and Singhai 2021), thus prompting the scientific community to look for some other potential climate drivers of ISMR.

Secondly, there is a growing recognition for the role of Tropical Atlantic SST anomalies as an important driver of interannual ISMR variability (Kucharski et al. 2008, 2009; Wang et al. 2017; Pottapinjara et al. 2021; Sabeerali et al. 2019). Tropical Atlantic SSTs exhibit two dominant modes: the Atlantic Zonal Mode (AZM or Atlantic Niño), which takes place along the Equator and the Northern Tropical Atlantic (NTA) mode focusing on SST fluctuations off the Equator (e.g., Yang et al. 2018, 2021; Ren et al. 2021). Note here that the NTA is also known as the northern part of the Atlantic Meridional Mode (AMM; e.g., Chiang and Vimont 2004; Yang et al. 2018; Cabos et al. 2019), with the NTA playing a leading role in its time variations (e.g., Jiang and Li 2021). The AZM primarily peaks during the boreal summer (June–August) and over the cold tongue region of the eastern equatorial Atlantic and off the southwestern African coast (e.g., Zebiak 1993; Xie and Carton 2004). The subsequent studies show an inverse relationship between the AZM and ISMR, leading to strengthening (weakening) of ISMR during cold (warm) phases of AZM (Kucharski et al. 2008, 2009; Wang et al. 2009; Pottapinjara et al. 2021; Sabeerali et al. 2019). However, several studies showed a limited influence of AZM on ISMR as both interact with ENSO in a complex manner (Ding et al. 2012; Terray et al. 2023). Consistent with this, the correlation between AZM and ISMR is also found to be very weak for the recent period (0.04 for the period 1979–2017) and further its influence on ISMR is projected to weaken under global warming (Sabeerali et al. 2022).

The NTA SST anomalies typically peak in boreal spring (March–May, MAM) (Czaja et al. 2002; Yang et al. 2018). The NTA SST anomalies usually arise from the surface wind-evaporation feedback involving (northeasterly) trade winds and turbulent surface latent heat fluxes (e.g., Yang et al. 2018, 2021), which are dominantly induced by external forcings, such as ENSO and the North Atlantic Oscillation (NAO). However, as ENSO forcing is mediated via tropical and extratropical teleconnections (e.g., García-Serrano et al. 2017; Jiang and Li 2019; Park and Li 2019), disentangling the respective roles of ENSO and NAO on NTA variability is challenging. The NTA SSTs forced by ENSO can also be interpreted as a delayed negative feedback by accelerating the demise of ENSO and hence further enhancing ENSO biennial variability (e.g., Wang et al. 2017). Thus, the NTA SSTs may also serve as an ENSO precursor (Ham et al. 2013a, b). As NTA SSTs peak in MAM, it is also worth exploring their role on ISMR and the space–time evolution of the whole ENSO–ISM system, which is otherwise not well explored in the literature. There are only a few studies in this direction and the underlying physical processes are not well understood and hence remain controversial (Rong et al. 2010; Vittal et al. 2020; Terray et al. 2023).

In short, most of the earlier studies have focussed on the direct forcing of AZM on ISM, as AZM is considered to be largely independent of ENSO and, thus, can be an additional driver of ISM variability beyond ENSO. However, its links to ISM are strongly modulated at decadal time scales with a weaker association in the recent period (Ding et al. 2012; Terray et al. 2023). On the other hand, the NTA is a key-driver of biennial variability in ENSO due to its capacitor effect (Ham et al. 2013a, b; Wang et al. 2017) and hence emerges as a new precursor for the whole ENSO–ISM system, but again the underlying physical processes need further investigations. The teleconnection pathways linking NTA to ISMR, mediated by ENSO (here and after "NTA–ENSO–ISM" relationship), are therefore illustrated in the present study using observations, coupled model simulations and dedicated coupled sensitivity experiments. The overall objective is to bring deeper physical insights and new perspectives on the NTA–ENSO–ISM system.

Section 2 outlines the datasets and simulations used, the design of our sensitivity experiments and the methodology adopted. Section 3 describes results from the observations and reanalysis. Section 4 discusses the results from a control simulation and the sensitivity experiments. Section 5 finally summarizes the main conclusions with a discussion.

2 Data, methods, and numerical experiments

2.1 Observed data

We used two different observed rainfall products to study the NTA–ENSO–ISM relationship. Firstly, we considered the high-resolution ($0.25° \times 0.25°$) quality-controlled gridded

precipitation dataset from the India Meteorological Department's (Pai et al. 2014), for the period 1979 to 2017. Secondly, we used a monthly mean precipitation dataset with a horizontal resolution of 2.5° × 2.5°, as obtained from the Global Precipitation Climatology Project (GPCP) monthly precipitation analysis for the period from 1979 to 2019 (Adler et al. 2018). For assessing the observed SST teleconnection patterns associated with the NTA–ENSO–ISM system, we used the Met Office Hadley Centre Sea Ice and Sea Surface Temperature (HadISST) dataset (Rayner et al. 2003). We also used the ERA5 dataset of the European Centre for Medium-Range Weather Forecasts (ECMWF; Hersbach et al. 2020) for documenting the associated atmospheric signatures. Specifically, the three-dimensional atmospheric circulation parameters [i.e., horizontal and vertical components of velocity, and mean sea level pressure (MSLP)] are taken from ERA5. The observed diagnostics are performed for a common period of 1979–2017.

2.2 Methodology

For this analysis, all the observed and simulated datasets are analysed at monthly time scale and are detrended by removing a linear fit to the data at each location over the full observed data record. Note that the results are not sensitive to the applied detrending. All the datasets are also converted into 1° × 1° resolution to foster a direct comparison between observations and simulations.

In order to monitor the time variations of the ENSO–ISM system, we defined two standard indices: (a) the Nino 3.4 index as monthly SST anomalies averaged over the region, 5° S–5° N and 170° W–120° W; and (b) the ISMR time series as rainfall anomalies averaged over the land points in the region, 70° E–95° E and 10° N–30° N for the JJAS season.

The observed El Niño (La Niña) years are identified by the Oceanic Niño Index (ONI) (3-month running mean of SST anomalies in the Nino 3.4 region) being above 0.5 °C (below − 0.5 °C) for a minimum of five consecutive seasons (i.e., from June to August until October to December). We also ensured that the identified ENSO events start develop in the boreal summer (JJAS) before attaining peak in the following boreal winter. The identified ENSO events (see Table 1) are consistent with the list of ENSO events in https://origin.cpc.ncep.noaa.gov/products/analysis_monitoring/ensostuff/ONI_v5.php.

On the other hand, the identification of NTA events is based on the dominant SST mode through Empirical Orthogonal Function (EOF) analysis (for both the observed and simulated datasets) as applied over the NTA region (70°W–10° W and 0°–30° N), following Yang et al. (2018) and Ren et al. (2021). Based on the seasonality characteristics of NTA SST anomalies (see Sect. 3.1 for a detailed description on the NTA SST seasonal cycle), we applied the EOF analysis on detrended SST anomalies over the NTA region during the period from March to May (MAM). The normalized Principal Component (PC) time series of the first EOF mode is then used to derive the cold and warm NTA events (for both observed and model data), based on the threshold of one standard deviation (SD). It's worth noting from Table 1 that cold (warm) NTAs (as identified during MAM) preceding the La Niña (El Niño) events are almost absent, while cold (warm) NTA events preceding the El Niño (La Niña) events is the rule in general. These years (see Table 1) with a consistent NTA–ENSO evolution, are then used to prepare composite maps for the seasonal evolution in a 2-year window from September (− 1) to November (− 1) [SON(− 1)], December (− 1) to February (0) [D(− 1)JF(0)], March(0) to May(0) [MAM(0)], June(0) to September(0) [JJAS(0)] and October(0) to December(0) [OND(0)], where − 1 represent the year preceding the peaks of the index (used to define the composites) and 0 represent the year of the peaks.

A two-tailed Student's *t*-test with unequal variances is also employed to establish the statistical significance of all the composites, for both the observed and model datasets

Table 1 Statistics of ENSO and NTA events in observation

El-Nino Years	La-Nina Years
1982,**1986**,**1987**,**1991**,**1994**,1997,2002, 2004,2006,**2009**,**2014**,**2015**	**1983**,1984, **1988**,1995,**1998**,1999,2000, **2005**,2007,2008,**2010**,2011
Cold NTA Years	Warm NTA Years
1985,1986,1989,1991,1992,1994,2009, 2012,2014,2015	1980,1981,1983,1987,1988,1998,2005, 2010

In the first row of the table, the cold and warm NTAs preceding the El-Niño and La-Niña events are highlighted in blue and red, respectively. Following similar convention, we also marked the only one warm NTA event preceding the El-Niño events, in red. As the cold NTA events preceding the La-Niña events are absent, it is not highlighted. See Sect. 2 for the identification procedure

(Storch and Zwiers 2002). A two-tailed Student's *t*-test is further used to assess the statistical significance of the correlation analysis.

2.3 Simulations and sensitivity experiments using the IITM-ESM coupled model

An important difficulty in assessing the NTA–ENSO–ISM relationship is the complexity of the pairwise interactions between the three components of this system due to the tight inter-basin linkages between the tropical Pacific, Atlantic and Indian oceans (Cai et al. 2019; Terray et al. 2021; 2023). This implies that it is difficult to delineate the specific processes (i.e., causes and effects) underlying the NTA–ENSO–ISM relationships solely based on observations. This prompted us to use a global coupled model, which is presently one of the best numerical tools available to demonstrate the NTA impact on the ENSO–ISM system, despite its inherent biases (e.g., Sperber et al. 2013; Prodhomme et al. 2014; Terray et al. 2018). The selected coupled model is the IITM Earth System Model (IITM-ESM), which is developed at the Indian Institute of Tropical Meteorology (IITM) (Swapna et al. 2018) and subsequently contributed to the sixth phase of the Coupled Model Intercomparison Project (CMIP6, Eyring et al. 2016).

The atmospheric model used in IITM-ESM is the Global Forecast System (GFS) at a spectral resolution of T62 with 64 sigma-pressure hybrid levels and top model layer extending up to 0.2 hPa (Moorthi et al. 2001). Its land component is NOAH-LSM consisting of four soil layers, 13 vegetation types and nine soil types (Ek et al. 2003). Its oceanic component is the NOAA/GFDL Modular Ocean Model Version 4p1 (MOM4p1; Griffies 2009). It has 0.25–1° horizontal resolution, 50 vertical levels and includes a sea-ice model. The atmosphere and ocean exchange quantities such as heat and momentum fluxes, every half an hour, with no flux adjustment. The IITM-ESM simulates the ISM mean state, ENSO, IOD and ISM variability reasonably well, with a realistic ENSO–ISM relationship (Swapna et al. 2018). Figure S1 further substantiates its performance for the ENSO variability and its seasonality.

First, we have used the last 200 years of a very long (~ 500 years) preindustrial climate control simulation (here after Pi-Control) to further understand and illustrate the robustness of the NTA–ENSO–ISM association in the background of internal variability of the climate system. This Pi-Control simulation uses the GHG concentrations, solar irradiance, anthropogenic aerosols and land-use-land-cover conditions of 1850 following CMIP6 protocol for the preindustrial climate simulations.

Note that an alternative is to use historical simulations containing all the forcings (e.g., both natural and anthropogenic) to ascertain the observational results as the observed climate system is also experiencing the anthropogenic forcings. But, assessing the robustness of the NTA–ENSO–ISM relationship in the presence of both the anthropogenic and natural forcings is even more complicated, as the signature of natural variability may be masked by the strong anthropogenic forcings during the historical period (e.g., Nath et al. 2018). So, we prefer to examine the robustness of our results in the perspective of unforced natural variability of climate system, i.e., using a very long Pi-Control simulation, in which the role of internal variability is reduced. This choice is also justified by the fact that the Pi-Control simulation allows us to increase drastically the number of short sensitivity runs we can perform with our numerical protocol as described later in this session.

In order to identify ENSO and NTA events in the Pi-Control run, we used the same approach as in observations, but with a different threshold (i.e., 1 °C) for the ENSO events. The statistics of the simulated ENSO and NTA events are provided in Table 2. Interestingly, the Pi-Control also shows the tendency of NTA events to be associated with a biennial rhythm in the simulated ENSO and to precede the ENSO events of opposite polarity, as in observations (compare Tables 1 and 2).

Secondly, we performed a set of dedicated sensitivity experiments using the IITM-ESM coupled model to infer the precise role of the pre-monsoon NTA SST anomalies in the evolution of the whole ENSO–ISM system. For these sensitivity experiments, we adapted the pacemaker experimental design of Kosaka and Xie (2013) by imposing observed SST anomalies in the North Tropical Atlantic (i.e., NTA domain:

Table 2 Statistics of ENSO and NTA events in Pi-Control simulations

El-Nino	La-Nina
32	35
Cold NTA	Warm NTA
31	31
Cold NTA preceding El-Nino	Warm NTA preceding La-Nina
10 (8 is forced by previous La Nina)	11 (9 is forced by previous El Nino)
Cold NTA forced by previous La Nina	Warm NTA forced by previous El-Nino
19	20

70° W–10° W and 0°–30° N) in the coupled model. The recent CMIP6 simulations also followed a similar experimental design for the so-called pacemaker experiments (see https://www.wcrp-climate.org/images/modelling/WGCM/CMIP/CMIP6-EndorsedMIPs_Summary_150819_Sent.pdf). The experiments include all forcing as used in CMIP6 Pi-Control simulation, and the observed SST anomalies are restored in the NTA domain. The SST signal is imposed by altering surface heat flux anomaly over the NTA region corresponding to both the warm and cold NTA events. The surface heat flux correction is obtained by considering a 50 m deep mixed layer depth following the equation $\Delta Q_{\text{net}} = \rho \times c_{\text{p}} \times H \times \Delta\text{SST}$, where ρ is the ocean density, c_{p} is the specific heat capacity of sea water, H is mixed layer depth, SST is Sea Surface Temperature (as defined earlier) and Q_{net} is the net surface heat flux. A similar methodology was followed by Gregory et al. (2016), which is referred to as the Flux anomaly forcing model Intercomparison project (FAFMIP) in CMIP6. It is important here to note that the ocean–atmosphere coupling is still active in the NTA in the sensitivity experiments. So, the NTA anomalies simulated in the sensitivity experiments can be different from the imposed (observed) NTA SST anomalies in contrast to other pacemaker experiments as done in previous studies (Ding et al. 2012; Kosaka and Xie 2013). In other words, these experiments are idealized ones to test the physics of the relationships and, more specifically, the eventual nonlinearity of the system, rather than to reproduce with fidelity of the observed evolution of the NTA SSTs. For these reasons, the correct reference for analyzing the results of these sensitivity experiments is not the observed datasets as in Ding et al. (2012) or Kosaka and Xie (2013), but the years extracted from the Pi-control simulation, which start from the same initial conditions as used in the sensitivity experiments as explained in more details below.

All the sensitivity experiments are performed here are ensembles of short 1-year integrations. To be more precise, 1-year simulations are performed for the following cases: four strong El Niño and four strong La Niña events as identified from the Pi-Control simulation (see Tables 2, 3). These different ENSO cases are selected by adhering to the criterion described above and accordingly these El Niño (La Niña) events start develop in the boreal summer (e.g., JJAS(0)) thus attaining maximum SST warming (cooling) in the following boreal winter. More precisely, the 67 ENSO events as identified from the composite analysis were arranged based on the descending order of their SST magnitudes (i.e., from highest to lowest magnitudes) and we selected the top 20% (with highest magnitudes) from this list of events. It is important to note here that, the selection is explicitly based on ENSO events with no reference to NTA events in the preceding or following MAM seasons. Thus, the selected events (i.e., top 20%) may or may not include a NTA SST signature before or after the ENSO events. Finally, the aforementioned eight strong ENSO events (out of the top 20%) are chosen subjected to the availability of corresponding restart files from the Pi-Control simulation. The sensitivity experiments start from the selected El Niño (La Niña) mature state in January Initial Conditions (ICs) with an intention to simulate the La Niña (El Niño) transitions in the subsequent seasons (i.e., boreal summer). To be precise, suppose an arbitrary year (e.g., yr) is identified as developing El Niño (La Niña) phase in the Pi-Control and so the sensitivity experiments are started from the January IC corresponding to the El Niño (La Niña) mature phase at yr + 1. Accordingly, four 1-year simulations are done starting from strong El Niño ICs (i.e., from January ICs) and by imposing warm SST anomalies over NTA region by altering surface heat flux anomaly over the NTA region. Similarly, four 1-year simulations using strong La Niña ICs have been done by imposing cold NTA SST anomalies. The ensemble means of the runs with warm and cold NTA SSTs imposed are referred as warmNTA_ElNinoIC_EXP and coldNTA_LaNinaIC_EXP, respectively.

In order to assess objectively the significance of the imposed NTA warm or cold SST anomalies in these ensembles of short 1-year simulations, we also computed the ensemble means from the years in the Pi-Control starting with the same ICs as used for each set of the sensitivity

Table 3 Summary of the numerical experiments done as performed using IITM-ESM

Name of the experiment	Description	SST imposed area	Length of simulation	Number of ensembles
Pi-Control	Following CMIP6 protocol for the preindustrial climate simulations (taken from CMIP6 data portal)	None	200 years	None
warmNTA_ElNinoIC_EXP	Warm SST anomalies are imposed over NTA region, using strong El Niño initial conditions (ICs) as identified from the Pi-Control (see text for more details)	NTA region: 70°W–10°W and 0°–30°N	1 year	4 (i.e., 4 ensemble runs using strong 4 El-Niño ICs)
coldNTA_LaNinaIC_EXP	Cold SST anomalies are imposed over NTA region, using strong La Niña ICs as identified from the Pi-Control	Same as above	1 year	4 (i.e., 4 ensemble runs using strong 4 La-Niña ICs)

experiments (i.e., using the years in the Pi-Control starting from the four El Niño and four La Niña ICs as used in the sensitivity experiments). In the following, we will refer to these ensemble averages from the Pi-Control as ElNinoIC_PiCNTL and LaNinaIC_PiCNTL, respectively. The results from the sensitivity experiments are then statistically compared with these ensembles averages derived from the Pi-Control. In other words, we computed the following ensemble mean differences: warmNTA_ElNinoIC_EXP minus ElNinoIC_PiCNTL and coldNTA_LaNinaIC_EXP minus LaNinaIC_PiCNTL. A two-tailed Student's *t*-test is further used to assess the statistical significance of these differences at the grid-point level (Storch and Zwiers 2002).

The overall goal of these different sets of experiments is to detect if the imposed NTA SST anomalies in each set are susceptible to modulate the whole ISM–ENSO system, or only one of the components of this system after the ENSO peaks and, more importantly, to highlight the possible nonlinearity of this system with respect to the polarity of the imposed NTA SST anomalies. This question has not been well explored in past modeling studies, despite the observations clearly suggest such nonlinearity as illustrated in the following section.

3 Results

3.1 Dominant observed modes of NTA SST variability

As a first step to assess the NTA–ENSO–ISM relationships in observations, we identified the leading mode of NTA SST variability by applying the EOF analysis to annual mean SST anomalies over the region bounded by the longitudes (70° W to 10° W) and latitudes (Eq to 30° N) as shown in Fig. 1a, b. Note that this leading SST EOF mode (i.e., EOF1, Fig. 1a) explains approximately 68% of the total variance and hence is well separated from the other modes (EOF2 describes only 8.7% of the total variance, figure not shown) following the rule of North et al. (1982). As the NTA SST variability is found to peak during MAM (see Fig. 1c), EOF analysis is also performed to the seasonal mean (MAM) SST anomalies over the NTA region (see Fig. 1d, e). In this case, the EOF1 mode explains 71% of the MAM SST variance (EOF2 accounts only for 7.1% of the MAM variance, not shown here). The dominant mode of NTA SST variability is characterized by a basin-wide SST warming (at its positive phase) with both leading EOFs (for annual as well as MAM season) showing good correspondence and the associated PCs showing a strong linear correlation of 0.89, significant at the 95% confidence level. This suggests that the dominant mode of SST variability over NTA region exemplifies during MAM.

The seasonal evolution of cold and warm NTA composites (as described in Sect. 2), based on the NTA events listed in Table 1, are shown in Fig. 2 from SON(−1) to OND(0) period. The NTA SST anomalies during both warm (cold) events initiate in boreal autumn and winter seasons (i.e., SON(−1) to D(−1)JF(0)), subsequently peak during boreal spring (MAM(0)) and persist till summer (JJAS(0)) period. Interestingly, these SST anomalies last for 2–3 seasons only and rapidly dissipate afterwards (Ham et al. 2013a, b). Some interesting nonlinear features can also be noted as the cold events emerge

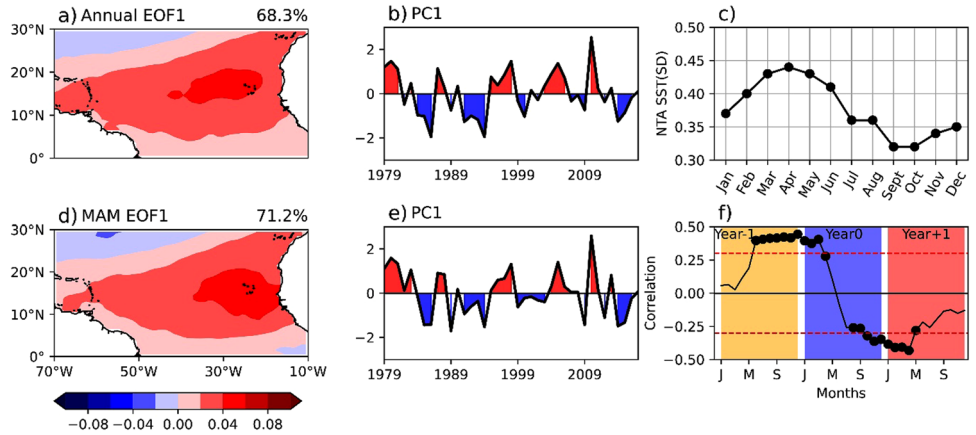

Fig. 1 Empirical Orthogonal Function 1st mode (EOF1) of detrended observed SST anomalies over the North Tropical Atlantic (NTA), using HadISST. (**a**) and (**d**), are EOF1 for annual, and March–May (MAM) period, respectively. (**b**) and (**e**), normalized Principal Component (PC1) corresponding to EOF1 for annual and MAM season, respectively. **c** Monthly Standard deviation (SD) of NTA. **f** Lead-Lag correlation between NTA SST Index (based on the normalised PC1 index for MAM season) and monthly Nino3.4 SST Index, starting from the beginning of the previous year (i.e., year − 1) to the end of the following year of the NTA (i.e., year + 1). In (**f**), black dots (red dotted lines), respectively, indicate the correlation values that are above the 90% (95%) significance confidence level according a two-tailed Student's *t*-test. In (**a**), (**c**) and (**d**), the unit is °C

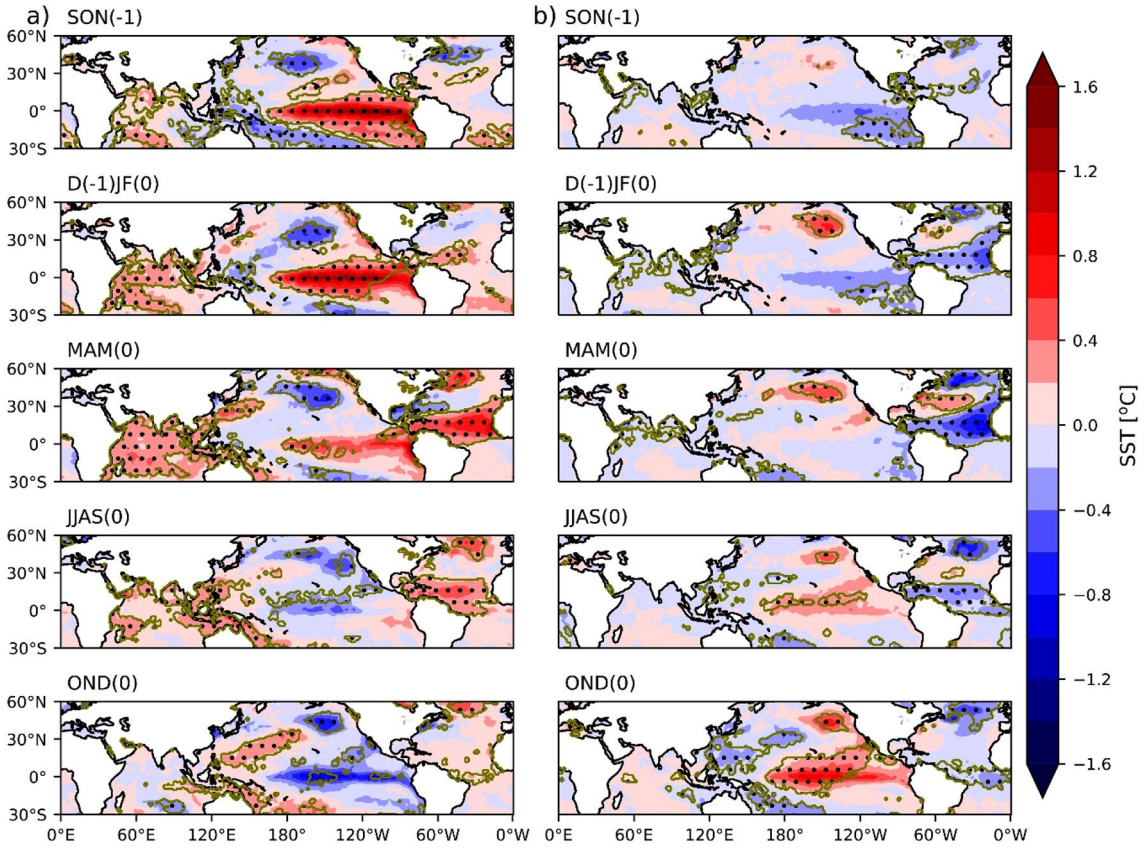

Fig. 2 Observed composite maps for the seasonal evolution in a 2-year window from SON(−1) to OND(0) using HadISST detrended SST anomalies for **a** warm NTA and **b** cold NTA events. warm and cold NTA events are based on the normalised PC1 index for MAM season (see Sect. 2 for more details). The stippling (olive contour), respectively, denotes the SST anomalies attaining 95% (90%) significance confidence level according to a two-tailed Student's *t*-test with unequal variances (Storch and Zwiers 2002)

in the eastern side of the NTA region while the warm NTA events are first detected in the western part of the NTA. Note that there are significant warm (cold, see Fig. 2) SST anomalies over the central to eastern Pacific during SON(−1) to MAM(0) seasons before warm (cold) NTA events. This indicates that many of the warm and cold NTA events during boreal spring may be initiated by the previous ENSO state itself, especially for the warm NTA events (García-Serrano et al. 2017; Jiang and Li 2019; Park and Li 2019; Terray et al. 2023). For more clarity on this, Fig. 1f shows the lead-lag correlations between NTA PC1 index (for MAM) and Nino3.4 SST monthly time series. It shows significant positive correlations 1 year before the NTA index thus exemplifying that most of the NTA events are dominantly forced by ENSO. Interestingly, the positive correlation gets reversed after the pre-monsoon season of year 0, attaining significance in the subsequent seasons (i.e., boreal summer to winter) before getting faded during the year + 1. This, in-turn, indicates the abrupt transition from El Niño to La Niña with the intervening NTA SSTs showing a precursory role (Ham et al. 2013a, b). As per earlier studies, this NTA forcing on ENSO can be interpreted as delayed negative feedback, thus opposing the ongoing ENSO events through the Atlantic capacitor effect (e.g., Wang et al. 2017; Terray et al. 2023), which further demonstrates the tight mutual interactions between the Pacific and Atlantic basins (Cai et al. 2019). While the effect of the ENSO during the preceding boreal winter and the possible precursory role of NTA on the ENSO evolution during year 0 is nicely illustrated by this simple correlation analysis, it should be also noted that these ENSO–NTA teleconnections during a 2-year window are also significantly asymmetric in observations as highlighted by the composite analysis in Fig. 2. More precisely, the NTA warm (cold) events are more (less) influenced by the preceding ENSO phase, but have a weaker (stronger) relationship with the ongoing ENSO phase as seen by the shaded regions during OND(0), which corresponds to the peak season of the events (Fig. 2a, b). Such asymmetry cannot be identified by the correlation analysis, but it clearly suggests that the underlying physical processes linking NTA and ENSO may vary with the polarity of the signals (Ham and Kug 2015). These contrasted SST anomaly evolutions are further discussed in the following sections.

Having illustrated the importance of pre-monsoon NTA SSTs as a key-driver of ENSO variability (Ham et al. 2013a, b; Wang et al. 2017), one can easily envisage that the pre-monsoon SST anomalies over NTA region can also be a useful precursor for predicting ISMR of the subsequent season (JJAS(0)). However, a relevant question arises here, how to physically interpret the precursory characteristics of pre-monsoon NTA SSTs with respect to ISMR? Whether the ISMR is directly or indirectly linked to NTA SSTs in the context of the dominant ENSO–ISM relationship? Furthermore, in the context of the aforementioned asymmetric NTA–ENSO association, how NTA–ENSO–ISM relationship is getting modulated? Whether similar non-linearity will manifest in the NTA–ENSO–ISM relationship as well?

3.2 Searching for pathways linking NTA to ISM in observations

In order to address these questions, we performed additional composite analyses based on the identified ENSO and NTA events (see Table 1). From Table 1, one can note that there are about 18 NTA and 24 ENSO events in observations. Further inspection of Table 1 shows that many of the NTA events precede the ENSO events. In particular, 6 out 10 cold NTA events precede the El Niño events, while 5 out of 8 warm NTA events are followed by La Niña events, thus constituting 11 ENSO events out of the total sample of 24 ENSO events in observations. Accordingly, two types of NTA–ENSO composites are constructed: one for the El Niño events preceded by cold-NTA events (i.e., coldNTA_ElNino) and the other for La Niña events preceded by warm-NTA events (i.e., warmNTA_LaNina). Note that 1994 is a strong IOD event leading to excess rainfall over the ISM region thus nullifying the impact of ENSO (e.g., Chowdary et al. 2021) and, accordingly, this event is not considered for the cold NTA composite.

We noted above that most of the observed NTA events appear to coincide with ENSO events. So, the number of independently (i.e., ENSO-free) occurring NTA events are comparatively less in observations in order to draw any robust conclusions on their direct impact on ISM variation. Accordingly, the present study uses NTA associated ENSO events to focus on NTA influencing ISMR by modulating ENSO events. On the contrary, it is important to highlight that not all the ENSO events are associated with NTA events, as the NTA associated ENSO events constitute only half of the total ENSO sample of 24 cases (see Table 1). Accordingly, there are six El Niño and seven La Niña events which are not included in the above NTA associated ENSO composites (i.e., coldNTA_ElNino and warmNTA_LaNina). It is intuitive to further compute their composites in order to compare the results with the previous NTA–ENSO composites and to disentangle the role of NTA SSTs in ISMR variability.

3.2.1 Large scale ocean-atmospheric features associated with the coldNTA_ElNino composite

Seasonal evolution of composite in SST (left panel a) and rainfall (right panel b) anomalies from boreal winter to autumn period (D(−1)JF(0) to OND(0)) during the coldNTA_ElNino are shown in Fig. 3. Figure 3a, in general, depicts the well-known ENSO life cycle in SST anomalies over the Pacific, with the El Niño developing phase occurring around boreal summer period and with a peak phase during boreal winter. Consistent with Fig. 2b, significant ENSO induced cold SST anomalies starts emerging over the NTA region during boreal winter of year − 1 (e.g., Jiang and Li 2019; Park and Li 2019; Terray et al. 2023), which grows in magnitude attaining peak values during boreal spring (i.e., during D(−1)JF(0) to MAM(0)) before getting dissipated in OND(0). There are significant SST anomalies over the North Pacific, which may also serve as an ENSO precursor (e.g., Vimont et al. 2003; Alexander et al. 2010; Terray et al. 2016; Ogata et al. 2019), in addition to the NTA SST anomalies.

The associated rainfall evolution in Fig. 3b for coldNTA_ElNino shows anomalous suppressed convection over the equatorial Atlantic during MAM(0) and JJAS(0), which can be induced locally by the NTA cooling or remotely by the emerging El Niño rainfall signature in the Pacific and the atmospheric bridge (Alexander et al. 2002). To be more precise, with respect to the NTA cooling during boreal winter and spring seasons, below normal rainfall anomalies are clearly visible over the off-equatorial NTA region (between Equator and 10° N) and positive rainfall anomalies are confined to the south of the Equator (see Figs. 3b, S2a,b) suggesting a possible role of local meridional SST gradients in triggering the local rainfall response in addition to remote ENSO forcing (Amaya et al. 2017; Cabos et al. 2019). As, the climatological Atlantic Intertropical convergence Zone (ITCZ) is observed to straddle over the equator during these seasons (Fig. S2a; Yang et al. 2018), the cold NTA SST anomalies seem to induce a southward shift of ITCZ (Yang et al. 2018; Ren et al. 2021). This north–south dipole structure in rainfall is more apparent during MAM(0) than during JJAS(0) (Fig. 3b) and is reminiscent of the AMM as discussed in the Sect. 1.

MSLP and wind at 850 hPa from the coldNTA_ElNino composite are presented in Fig. 4. In the left panels of Fig. 5, we show similar temporal evolutions but for the velocity potential and divergent wind vector at 200 hPa, while the right panels show the East–West circulation averaged over the Equator to 30° N. The associated circulation response over the NTA region (see Fig. 4), during D(−1)JF(0) and MAM(0), shows strengthening of the northeasterly trade

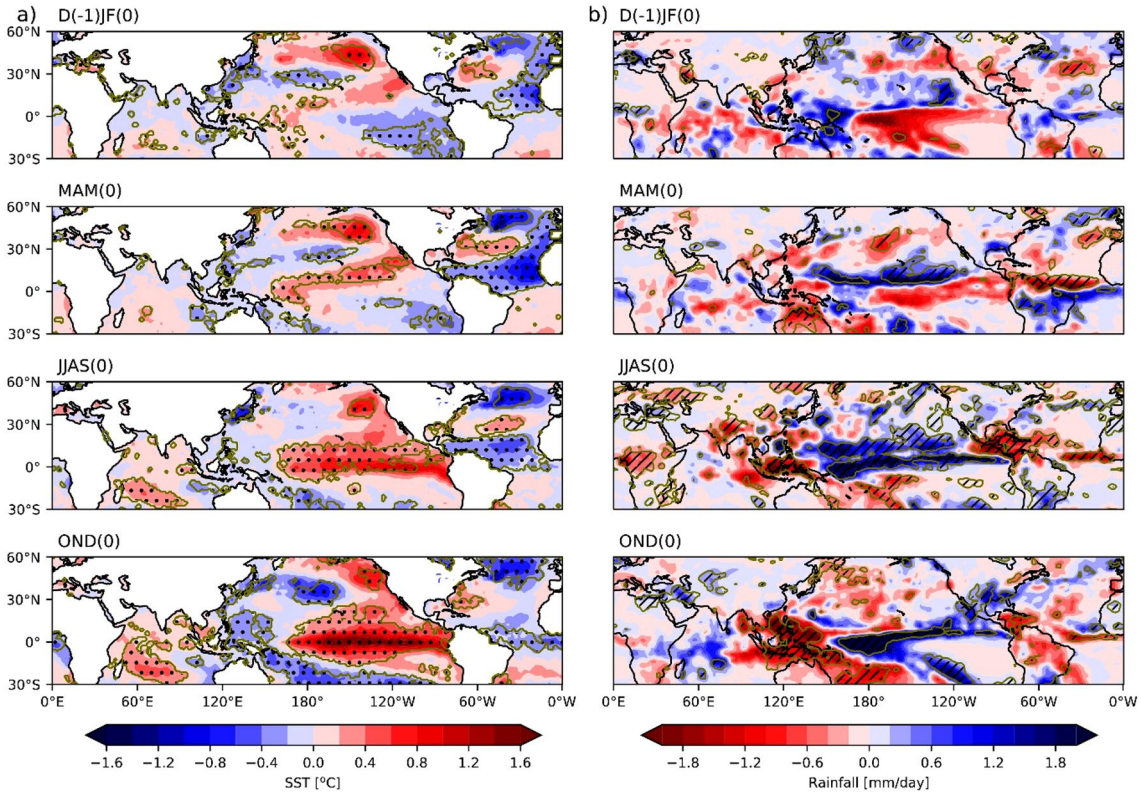

Fig. 3 Observed composite maps for the seasonal evolution in a 2-year window from D(−1)JF(0) to OND(0) for the coldNTA_ElNino composite as defined in Sect. 2. **a** HadISST and **b** GPCP rainfall anomalies, which are detrended. The stippling in (**a**) and black hatches in (**b**), indicate the anomalies attaining 95% significance confidence level according to a two-tailed Student's *t*-test with unequal variances (Storch and Zwiers 2002). The olive contours in both (**a**) and (**b**) indicate the same, but for the anomalies attaining 90% significance confidence level

winds emanating from the Azores High consistent with the possible role of the NAO in triggering cold NTA SST anomalies, in addition to ENSO. This in-turn increases the surface latent heat flux which further leads to the growth of the cold NTA SST anomalies, through wind–evaporation–SST feedback (WES; e.g., Amaya et al. 2017; Yang et al. 2018), from D(−1)JF(0) to MAM(0). However, the wind and SST anomalies dissipate quickly in boreal summer as soon as the Azores High polarity is reversed over the North Atlantic (Figs. 3a and 4). This suggests that the local WES feedback alone is not able to sustain the SST anomalies over the NTA after the observed anomalous peak in NTA SST during MAM(0), as described earlier (see Fig. 3a). Note that a similar WES feedback is also highlighted by earlier studies to trigger and sustain the AMM (Chiang and Vimont 2004; Cabos et al. 2019), which, in-turn, is dominated by the NTA (e.g., Jiang and Li 2021).

In addition to the well defined NAO signature during D(−1)JF(0) (Fig. 4), one can see distinct extra-tropical circulation features over the (North and South) Pacific Ocean, with alternating regions of anomalous low and high MSLP forming wave trains extending to mid-latitudes, which are reminiscent of the atmospheric Rossby wave response to equatorial convection over the Pacific warm pool (Trenberth et al. 1998). However, eventually associated with these anomalous wave trains or linked to the internal variability over the North Pacific, southerly/southwesterly wind anomalies emerge over the subtropical North Pacific during D(−1)JF(0) to MAM(0). This tends to weaken the Pacific trade winds, reduce the evaporation and, thus, induce SST warming over subtropical North Pacific with positive rainfall anomalies, during MAM(0) (Figs. 3, 4). During the same period (i.e., MAM(0), see Fig. 5), one can also see anomalous upper-level convergence accompanied by mid-level descending motion over the NTA region, with opposite anomalous circulation over the central tropical Pacific. This generates an anomalous east–west overturning circulation across the tropical Pacific and Atlantic Oceans, thus promoting enhanced convective activity and persistent westerlies over the western Pacific which further favour the emergence of El Niño warming conditions, but it is difficult to distinguish the respective roles of ENSO and NTA in this east–west overturning circulation as they are both used to define the composites described here. However, the

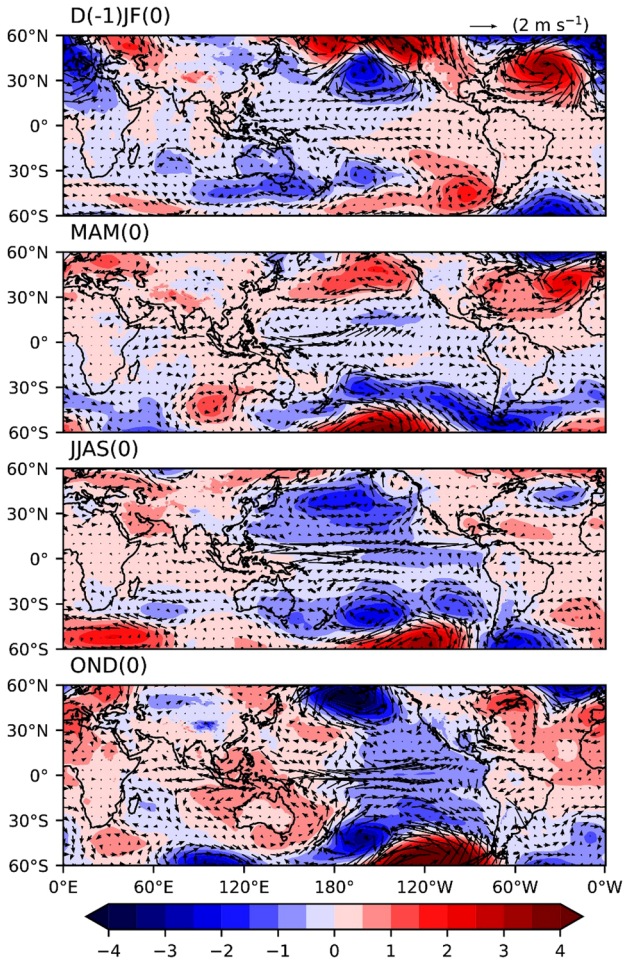

Fig. 4 Seasonal composite evolution maps (i.e., from D(−1)JF(0) to OND(0)) for the coldNTA_ElNino composite, as computed for MSLP (shading, hPa) and wind (ms^{-1}) at 850 hPa, using ERA5 dataset

cold NTA SST anomalies persists during JJAS(0) as well (Fig. 3a), so they can eventually contribute to the development of the Pacific warming conditions through this anomalous east–west circulation (Jiang and Li 2021).

As usually observed in a typical El Niño developing summer (e.g., JJAS(0)), one can see pronounced suppression (enhancement) of convection over the maritime continent (central to eastern equatorial Pacific), with the extended dryness over the Indian continent and neighbouring regions (Fig. 3b). In accordance with these, there is anomalous increase in MSLP over the Arid regions lying west of India, extending to Arabian Sea (50° E–70° E, 15° N–25° N), a concurrent weakening of the monsoon trough over the Indo-Gangetic Plain and a geostrophically consistent anomalous wind patterns suggesting a weakening of the monsoon Low Level Jet (LLJ; see Fig. 4 JJAS season). All these features in-turn imply a decrease in moisture transport (from Arabian Sea) to the Indian landmass as corroborated by an anomalous decrease in low-level moisture influx at 850 hPa (i.e., -3.6×10^{-3} m s^{-1} kg/kg) along the Arabian Sea longitude of 70° E (i.e., averaged between 7.5° N to 27.5° N). The weakening of the low-level monsoon flow is further reflected in the anomalous easterly divergent out-flow from the Pacific with upper-level convergence over the Indian monsoon region (see Fig. 5a).

In order to assess properly the possible impact of NTA on the "traditional" ENSO–ISM association**,** we now discuss the composites for El Niño events that are independent of NTA events (as described earlier, but figures not shown). The amplitude of the El Niño is mostly similar in both composites (i.e., with and without NTA events) and a well-defined El Niño SST pattern quickly emerges in JJAS, in both cases. However, the corresponding ISMR anomaly estimates in the El Niño composite without NTA show magnitudes of 0.5 mm day^{-1} for both GPCP and IMD, which is in contrast to the ISMR anomalies for the coldNTA_ElNino composite with both the rainfall products showing a stronger magnitude of 0.7 mm day^{-1}.

3.2.2 Response from the warmNTA_LaNina composite

As in the coldNTA_ElNino composite, the growth of warm NTA SST anomalies during D(−1)JF(0) to MAM(0) in the warmNTA_LaNina composite, is mainly through the modulation (i.e., weakening) of the trade winds over NTA region and the WES feedback (Fig. S3a,c). The emergence of warm SST anomalies over NTA region during D(−1)JF(0) to MAM(0) (Fig. S3a) is accompanied by a northward shift of the ITCZ, thus creating a north–south dipole structure in rainfall anomalies, but with a reversed polarity as expected (Figs. S2, S3). However, this north–south rainfall dipole and the associated WES feedback are observed to be less significant than in the coldNTA_ElNino composites. This suggests that the remote forcing, especially the one associated with the preceding ENSO is dominant here for explaining the weakening of the trade winds.

This El Niño-induced trade wind reduction can be explained in the following ways. First one is related to the anomalous low-level circulations associated with the El Niño-triggered extra-tropical response over the Pacific and Atlantic regions, but mediated by the Pacific–North American (PNA) pattern, during D(−1)JF(0) to MAM(0) (e.g., Wallace and Gutzler 1981; Jiang and Li 2019; see Fig. S3c). Second one is associated with the Rossby wave response to the El Niño-induced suppressed rainfall over the western equatorial Atlantic and Amazon basin (during the same period) which, in-turn, can trigger low-level cyclonic westerly flow over the NTA region (Gill 1980; García-Serrano et al. 2017) thus leading to the weakening of trade winds as well as to the growth of the warm NTA SST anomalies. Interestingly, these extratropical and tropical El Niño

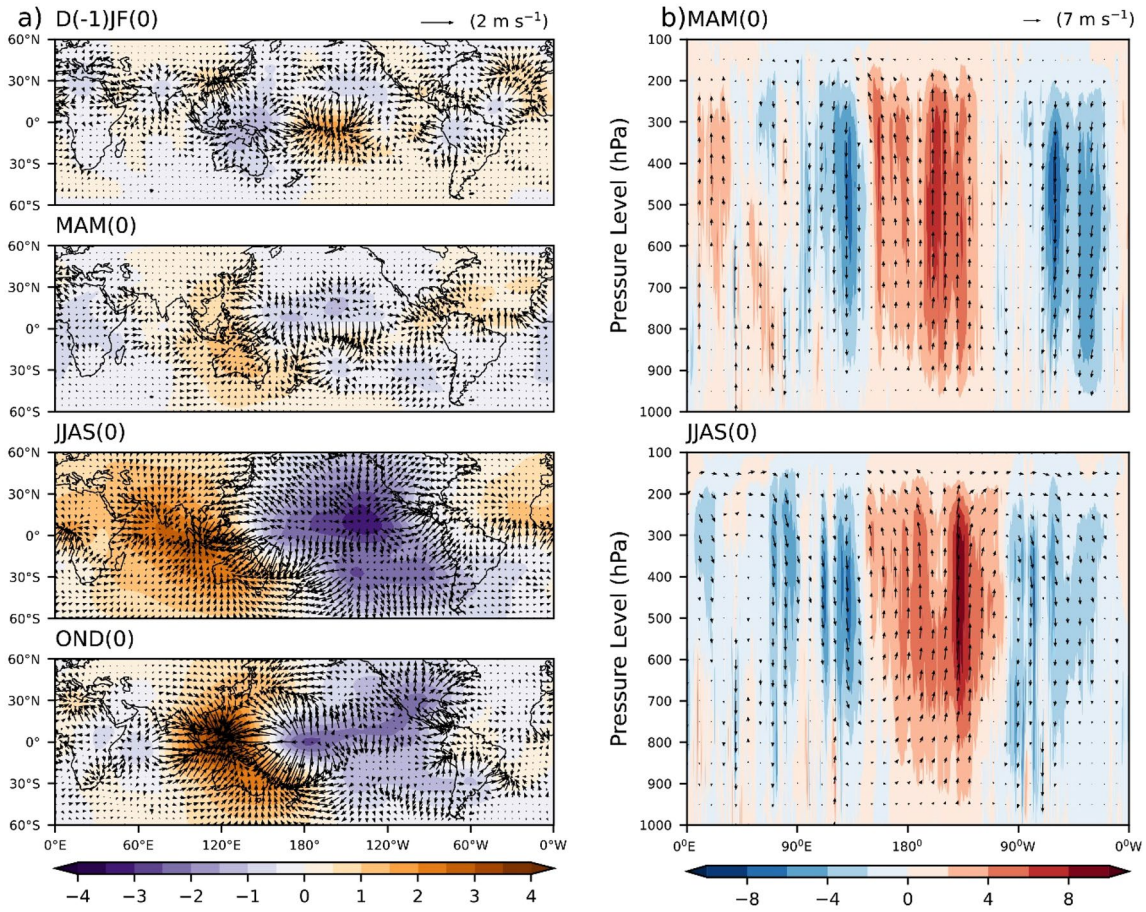

Fig. 5 Same as Fig. 3, but for **a** velocity potential (shading, $\times 10^6 m^2 s^{-1}$) and divergent wind vector (ms^{-1}) at 200 hPa, using ERA5 dataset. In **b** longitude-pressure cross-section of zonal wind (ms^{-1}) and vertical pressure velocity (Pas^{-1}) components, meridionally averaged over average over the Equator to 30°N, for MAM(0) and JJAS(0) seasons

forcings seem to dominate the warmNTA_LaNina composite, compared to the NAO forcing, as the North Atlantic MSLP patterns during D(− 1)JF(0) to MAM(0) (Fig. S3c) are found to be mostly induced by ENSO via PNA teleconnections (e.g., Cai et al. 2019). This is in contrast with the coldNTA_ElNino composite, which shows the role of both the previous La Niña and Azores High variability (e.g., NAO) in triggering cold NTA SST anomalies during MAM(0).

Over the tropical Pacific, during MAM(0), one can see the onset of easterly anomalies on its western end, possibly induced by NTA warm SST anomalies as suggested by Ham et al. (2013a, b). As per these studies, the NTA forcing, prominently induced by the preceding El Niño, can also lead to its fast demise and therefore acts as an Atlantic capacitor effect (e.g., Wang et al. 2017; Terray et al. 2023).

Consistent with a capacitor effect of both the Atlantic and Indian oceans, the warmNTA_LaNina composite during D(− 1)JF(0) also shows significant SST signatures in the equatorial Pacific and Indian Ocean regions (see Fig. S3), which is in strike contrast with its counterpart (i.e., coldNTA_ElNino, see Fig. 3), thus again revealing the non-linearity of the system probably owing to the key role of NAO in the coldNTA_ElNino composite.

During boreal summer (JJAS(0)), a decrease in MSLP can be seen over the Arabian Peninsula and Arabian Sea extending to the monsoon trough, which further results in the strengthening of the moisture transport to the Indian landmass (with an enhanced anomalous low-level moisture flux of 1.1×10^{-3} m s^{-1} kg/kg at 850 hPa, across the Arabian Sea longitude of 70° E) and thus causing above normal rainfall over the Indian region (see Fig. S3b–c). Interestingly, this anomalous increase in moisture incursion along the Arabian Sea during the warmNTA_LaNina composite is surprisingly less than the corresponding moisture flux estimated from the cold NTA counterpart (-3.6×10^{-3} m s^{-1} kg/kg), thus suggesting a non-linear response, as also recently found in Chakraborty and Singhai (2021), despite the Pacific SSTs during JJAS(0) show almost equal amplitudes for both the warm and cold NTA composites (i.e., the Nino3.4 SST

anomalies show 0.63 °C for coldNTA_ElNino vs − 0.69 °C for warmNTA_LaNina composites).

Importantly, the La Niña composites without NTA SST signature (figures not shown), show pronounced cooling over the equatorial Pacific during D(− 1)JF(0), which persists throughout the year until OND(0), thus manifesting themselves as multi-year La Niña events. In contrast, the warmNTA_LaNina composite show strong El Niño signal during D(− 1)JF(0) (see Fig. S3a) which gets completely transitioned to La Niña during subsequent JJAS period, again illustrating the efficiency of the Atlantic capacitor effect on ENSO consistent with previous studies (e.g., Wang et al. 2017). The ISMR response is also not similar in both composites (i.e. La Niña composites with and without NTA events). In particular, the NTA associated La Niña events (i.e., warmNTA_LaNina, see Fig. S3b) show more homogenous rainfall response over Indian landmass, in contrast to the La Niña composite without NTA events (figure not shown). Accordingly, the corresponding ISMR anomaly estimates in the NTA independent La Niña composite show modest value of 0.32 (0.23) mm day^{-1} from GPCP (IMD) which is in contrast to that of 0.7 mm day^{-1} (from both GPCP and IMD) for the warmNTA_LaNina composite. So ultimately, one can infer that this is again a manifestation of the modulation of ENSO–ISM teleconnections as intervened by NTA SSTs, with a fast El Niño to La Niña transition from boreal winter to summer (D(− 1)JF(0) to JJAS(0)) thus providing favourable conditions for the occurrence of a strong ISMR in the warmNTA_LaNina composite.

Obviously, it is difficult to delineate the causes and effects underlying the NTA–ENSO–ISM relationship using only observations. Hopefully, the dedicated sensitivity experiments (described in Sect. 2.3) can be useful to disentangle these processes, but before that we need to assess the NTA–ENSO–ISM relationship in the Pi-Control simulation.

4 Results using IITM-ESM coupled model

4.1 NTA–ENSO–ISM association in the Pi-Control simulations

In this section, we used a Pi-Control coupled simulation (i.e., using IITM-ESM) so as to test the robustness of the results in observations and thus to illustrate the NTA–ENSO–ISM relationship using larger data samples. We first assessed the performance of the coupled model in simulating the NTA SST variability and its relationship with ENSO. In Pi-Control, the leading SST EOF mode (EOF1) over NTA during MAM explains approximately 50% of the variance and is also well separated from the EOF2, which explains only 10% of the variance (see Fig. 6a, b, EOF2 is not shown). Both the observations and coupled model depict anomalies of uniform polarity over the entire NTA region for its leading modes (with a pattern correlation of 0.82), however, the coupled model is slightly underestimating the described variance by this mode, i.e., 50% against 71% in observations. Further the IITM-ESM reasonably well captures the observed seasonal peak of NTA SST variability during MAM(0), but the NTA SST variability is exaggerated during boreal summer as compared to observations (see Fig. 6c). The coupled model also simulates realistically the lead-lag relationships between NTA SSTs and ENSO, but the relationship of NTA SST anomalies to the previous ENSO state is significantly exaggerated compared to observations (see Fig. 6d). Most of the simulated NTA events during MAM(0) seem to be initiated by previous ENSO conditions, as illustrated by significant positive correlations during boreal winter (D(− 1)JF(0)) preceding the NTA index. This coincides with the observed inferences, but the intensity of this link to the previous ENSO condition is almost double compared to the observations (Figs. 1f, 6d).

Figure 7 shows the seasonal evolutions (i.e., from D(− 1)JF(0) to OND(0)) of coldNTA_ElNino composites as constructed from the Pi-Control simulations. Similar to observation (Figs. 3, 4, 5), Pi-Control shows that the cold NTA events are initiated in boreal winter (D(− 1)JF(0)), with SST anomalies attaining maximum values around MAM(0) which rapidly gets dissipated after JJAS(0). Similar results can also be inferred from the warmNTA_LaNina composite (Fig. S4). Firstly, both the composites from Pi-Control (Figs. 7, S4) are able to capture the teleconnection patterns of NTA events with tropical SST anomalies as seen from the observations (Figs. 3, 4, 5) and illustrate that the simulated NTA events are also well associated with ENSO transitions. The associated atmospheric response shows that the stronger ENSO forcing on NTA in Pi-Control is mediated through both the extra-tropical and tropical pathways (Jiang and Li 2019). However, in contrast with the observed results, both these pathways dominate in the warmNTA_LaNina and coldNTA_ElNino composites, while the role of NAO forcing is weaker. Thus, the Pi-control is unable to simulate the observed non-linearity in the ENSO-NTA teleconnections (e.g., compare Figs. 7, 8, S4 with Figs. 3, 4, S3). One plausible explanation is that the IITM-ESM, similar to other coupled models, fails to simulate the observed positive ENSO skewness (figure not shown). However, we cannot rule out the other factors (e.g., NAO, mean bias etc.), which need to be addressed through a separate study with more detailed investigations.

Secondly, both the composites illustrate the pronounced biennial nature of the ENSO-NTA system in Pi-Control (Fig. 7a, S4a), thus robustly replicating the reversal of polarities in correlations in a 2-year window (Fig. 6d). Both the composites also show the abrupt ENSO transitions from MAM(0) to JJAS (0) (see Figs. 7a, S4a), but again

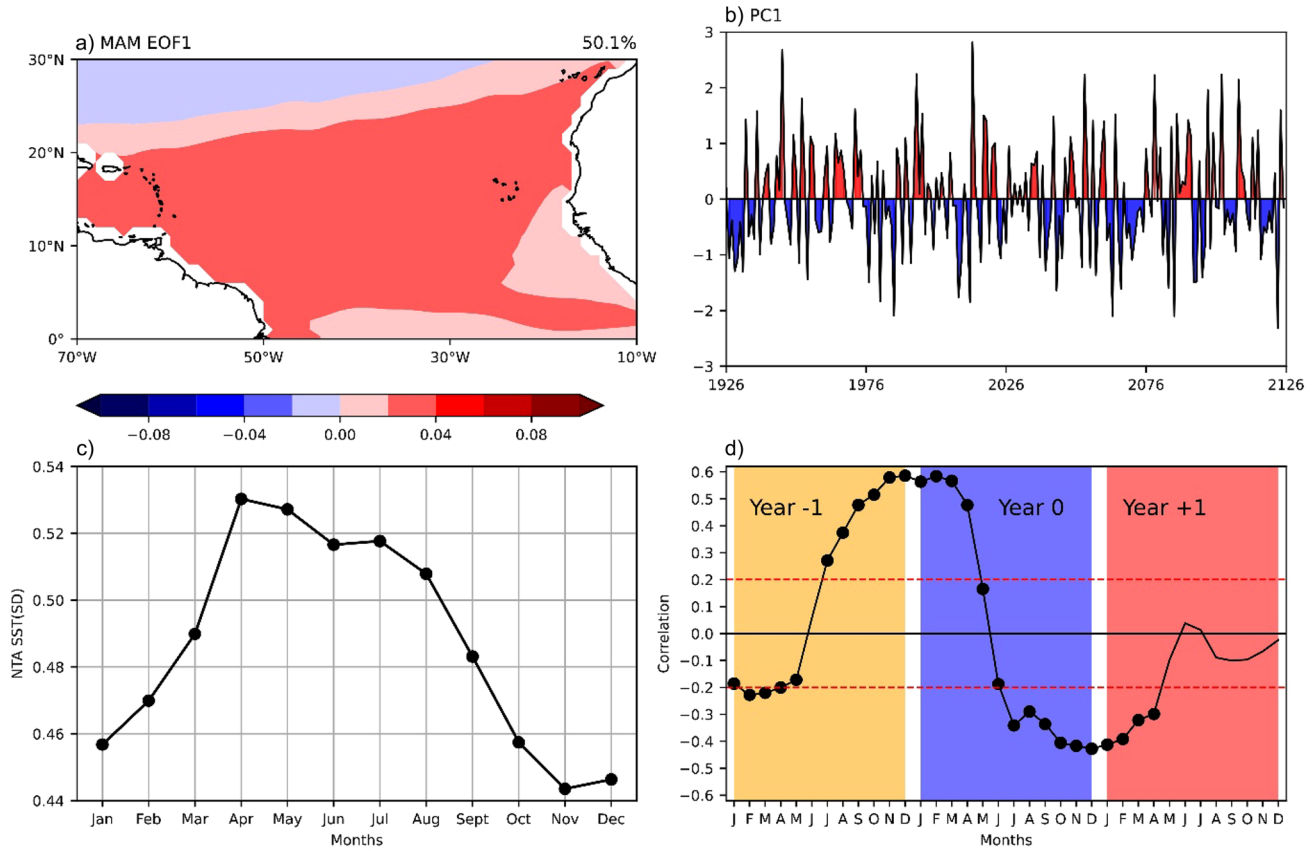

Fig. 6 EOF first mode of detrended SST anomalies over the North Tropical Atlantic (NTA) using Pi-Control simulation. **a** EOF1 for MAM SST anomalies (in °C). **b** normalized principal component (PC1) corresponding to EOF1 for MAM season. **c** Monthly SD of NTA (in °C). **d** Lead-lag correlation between NTA Index (based on the normalised PC1 index for MAM season) and monthly Nino3.4 SST Index, starting from the beginning of the previous year (i.e., year − 1) to the end of the following year of the NTA (i.e., year + 1). In (**d**), black dots (red dotted lines), respectively, indicate the correlation values that are above the 90% (95%) significance confidence level according a two-tailed Student's *t*-test

the precursory role of the NTA SSTs in this biennial system must be confirmed with the dedicated experiments in Sect. 4.2.

The associated anomalous rainfall and circulation characteristics (see Figs. 7, 8, S4) over both Pacific and NTA regions from the Pi-Control simulation are mostly similar to the observed features. In other words, significant ENSO-forced SST anomalies emerge over the NTA region during boreal winter and spring, accompanied by shift in ITCZ rainfall band and modulation of the trade winds. There are associated changes in the anomalous east–west overturning circulation over the tropical Pacific and Atlantic Oceans, potentially paving the way for the ENSO transition (Figs. 7, S4). In the ISM sector, Fig. 8a, b shows large-scale suppression (enhancement) of rainfall over the Indian landmass extending to the Bay of Bengal and maritime continent for the coldNTA_ElNino (warmNTA_LaNina) composites, respectively. Consistently, there is a weakening (strengthening) of the monsoon LLJ with anomalous upper-level convergence (divergence) over the Indian monsoon region (Figs. 7b, c, S4b, c). All these features are consistent with the aforementioned observed results.

Note, finally, that there are also some marked differences in results between observations/reanalysis and coupled model in the Atlantic sector. For example, though the NTA SST anomalies in the composites derived from observations and Pi-Control are very similar, the associated rainfall anomalies are not able to clearly depict the observed dipole structure in rainfall anomalies; i.e., significant observed rainfall anomalies north (south) of the equator for warmNTA_LaNina (coldNTA_ElNino) composites during boreal spring and early summer (see Figs. 3, S3; Figs. 7, S4 and Fig. 8). This may be probably linked with the coupled model bias in IITM-ESM as the simulated thermocline in Pi-Control is shallow compared to the observations (figure not shown) as in most current coupled models (Terray et al. 2023).

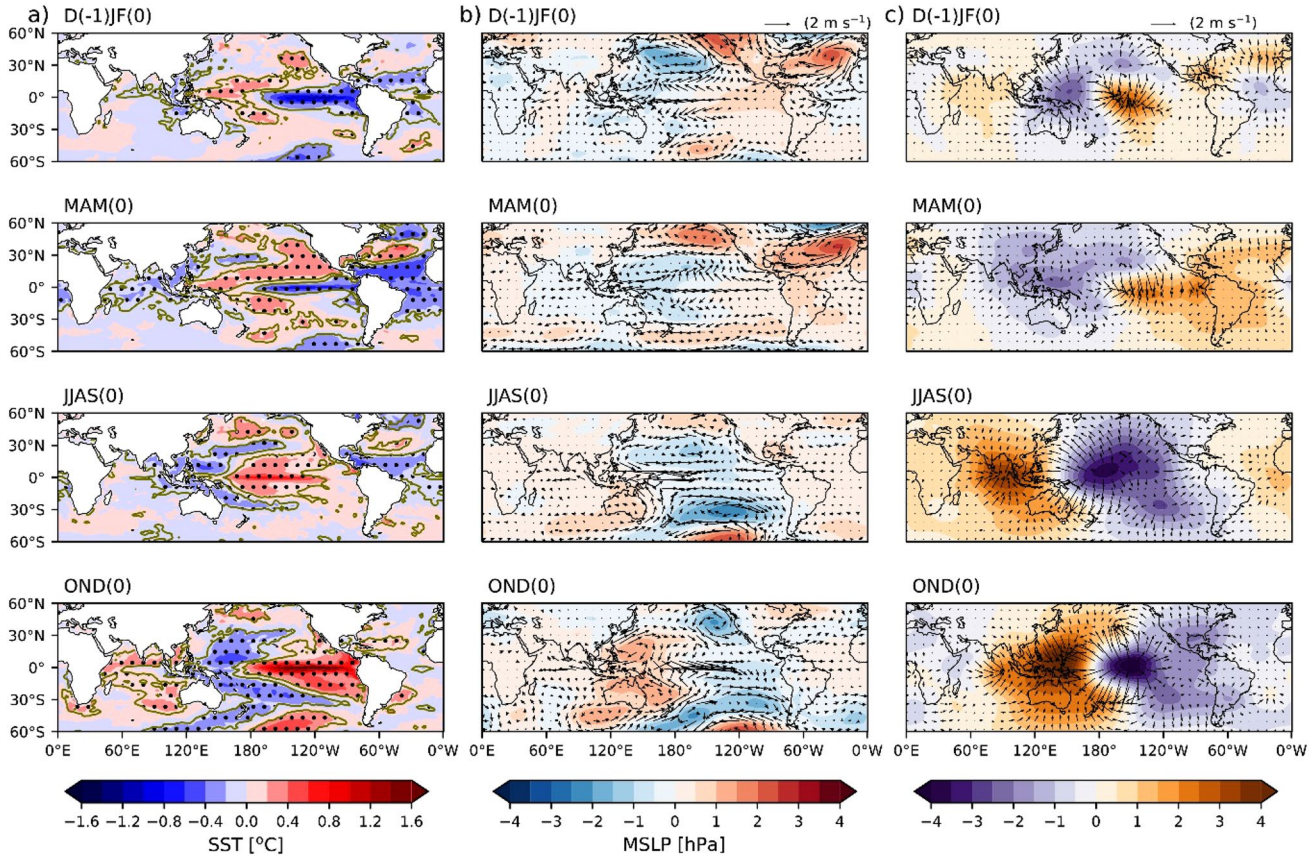

Fig. 7 Composite anomalous maps for the seasonal evolution in a 2-year window from D(−1)JF(0) to OND(0) for the coldNTA_ElNino composite as computed from the Pi-Control simulation (see Sect. 2 for more details). **a** SST (°C), **b** MSLP (shading, hPa) and Wind Vector at 850 hPa (m s^{-1}) and **c** velocity potential (shading, $\times 10^6 m^2 s^{-1}$) and divergent wind vector (ms^{-1}) at 200 hPa. In (**a**), black stippling (olive contour), respectively, indicate the SST anomalies attaining 95% (90%) significance confidence level according to a two-tailed Student's *t*-test with unequal variances (Storch and Zwiers 2002)

4.2 The NTA capacitor effect and its nonlinearity: insights from the sensitivity experiments

The relative success of Pi-Control in reproducing the observed lead-lag relationship between NTA and ENSO, as described in the previous section, is an important aspect as it qualifies the model for performing sensitivity experiments so as to test the hypothesis that the NTA SST anomalies can physically influence the evolution of ENSO–ISM. Note also that these experiments, by their designs, are not meant to represent the observed space–time evolution of the NTA events (as described in Sect. 2), but are useful to theoretically assess the possible impact of NTA SST anomalies on the evolution of ISM and ENSO, and to provide more insights on the physical processes involved.

The ensemble mean differences between the sensitivity and Pi-Control simulations (as described in detail at Sect. 2) for SST, rainfall and surface wind are shown in Figs. 9, 10 and 11. First of all, these figures generally illustrate the operation of the NTA capacitor effect and hence the remote teleconnections from NTA to ENSO conditions, as manifested by stronger ENSO SST signatures at OND(0); i.e., stronger La Niña (El Niño) peaks in warmNTA_ElNinoIC_EXP (coldNTA_LaNinaIC_EXP, see Fig. 9a, b) compared to Pi-Control. Next, it also reveals that, the amplitude of the local rainfall response (e.g., over the tropical Atlantic) for the imposed NTA SST perturbations is substantial and significant, and reveal a quick response to the imposed SST perturbation with a large enhancement (suppression) of rainfall over the NTA region collocated with warm (cold) NTA SST anomalous perturbation, as observed during boreal spring and summer season (see Figs. 9, 10), which is further consistent with our previous results, especially from the observations (e.g., see Figs. 3 and S3). As an illustration, the imposed warm SST over NTA for the El Niño IC experiment (i.e., warmNTA_ElNinoIC_EXP minus ElNinoIC_PiCNTL, see Figs. 9a, 10, 11a) is expected to induce horizontal SST gradients thus forcing low-level westerly wind to converge towards the region of warm SST perturbation, and hence causing the low-level moisture convergence

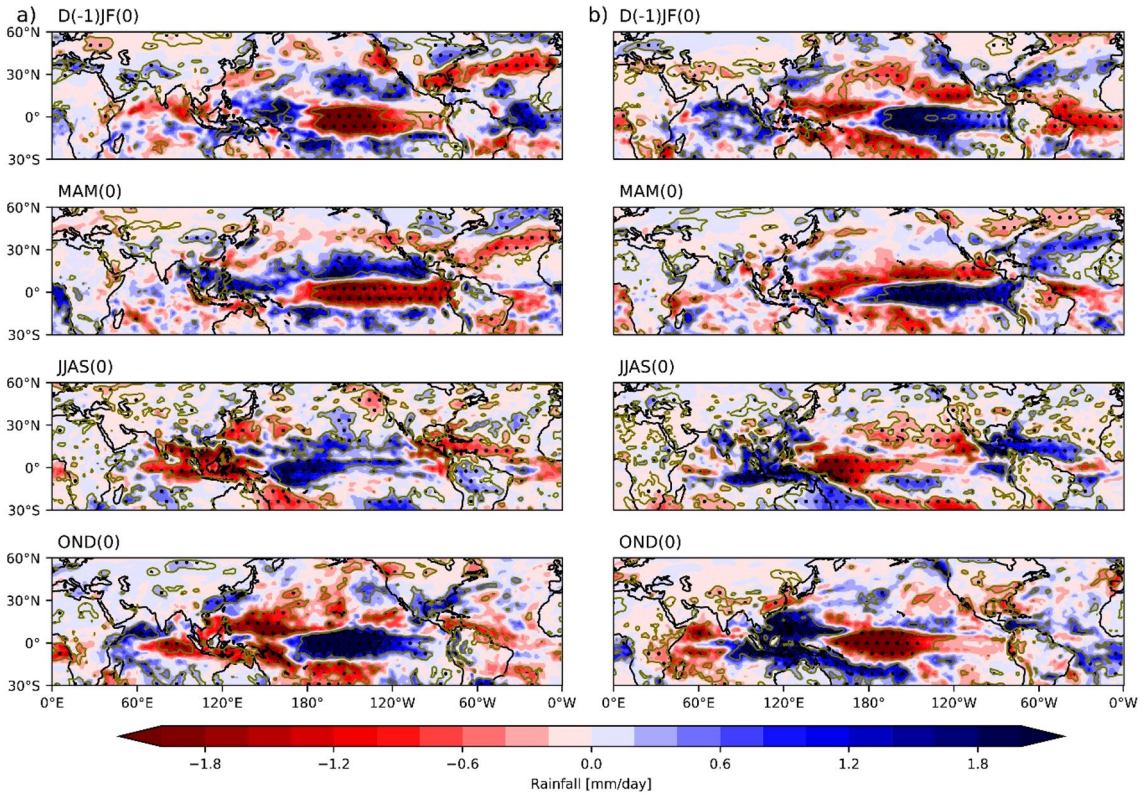

Fig. 8 Composite anomalous rainfall maps for the seasonal evolution in a 2-year window from D(−1)JF(0) to OND(0) as computed from the Pi-Control. Composite rainfall anomalies for **a** coldNTA_ElNino and **b** warmNTA_LaNina composites. Black stippling (olive contour), respectively, indicate the anomalies attaining 95% (90%) significance confidence level according to a two-tailed Student's t-test with unequal variances (Storch and Zwiers 2002)

and the associated rainfall enhancement over NTA region (Lindzen and Nigam 1987). Interestingly, the rainfall is largely supressed near the equatorial Atlantic suggesting a northward migration of ITCZ during boreal spring and summer season (see Fig. 10a), which is consistent with the observed results (Fig. S3) and, intriguingly, this is in contrast to the simulated features in Pi-Control (see Fig. 8b). Qualitatively, opposite linear responses are visible over the NTA region for the La Niña counterpart (coldNTA_LaNinaIC_EXP minus LaNinaIC_PiCNTL; see Figs. 10b, 11b).

Over the Pacific, one can however detect some non-linearity between the two experiments (compare left and right sides of Figs. 9, 10, 11). As soon as in MAM, significant warm SST anomalies emerge over the Pacific in coldNTA_LaNinaIC_EXP and these warm anomalies further amplify during JJAS (Fig. 9b). On the other hand, significant SST differences over the tropical Pacific in warmNTA_ElNinoIC_EXP emerge only during OND season (Fig. 9a). An interesting result from the sensitivity experiment is that the atmospheric response over the northeastern Pacific during MAM is very important to explain the changes in the Pacific in coldNTA_LaNinaIC_EXP. Stated distinctly, the results from coldNTA_LaNinaIC_EXP (relative to Pi-Control, see Figs. 10b, 11b) show suppressed rainfall and anticyclonic easterly anomalies over northeastern Pacific, which may be interpreted as an off-equatorial Rossby wave response to the decreased rainfall over NTA region (Ham et al. 2013a). Consistently, a low-level cyclonic flow is clearly seen over the tropical western Pacific during MAM and JJAS seasons in coldNTA_LaNinaIC_EXP (see Fig. 11b), thus creating El Niño initiating low-level westerlies over the western end of the Pacific which again resembles with the observed results (see Fig. 4), though the sensitivity simulations show an exaggerated amplitude in its atmospheric response. There is also an enhanced convective activity over the western Pacific (see Fig. 10b) during MAM and JJAS with reduced convection over the NTA during these periods (triggered by the imposed SST perturbation in the model) which is sufficient to generate an anomalous east–west overturning circulation across the tropical Pacific and Atlantic Oceans, thus promoting the El Niño conditions. In contrast, for the warmNTA_ElNinoIC_EXP, it shows only feeble wind response over the Pacific with the low-level easterlies emerging lately over the western Pacific (i.e., during JJAS period, see Fig. 11a) thus implying weaker La Niña response.

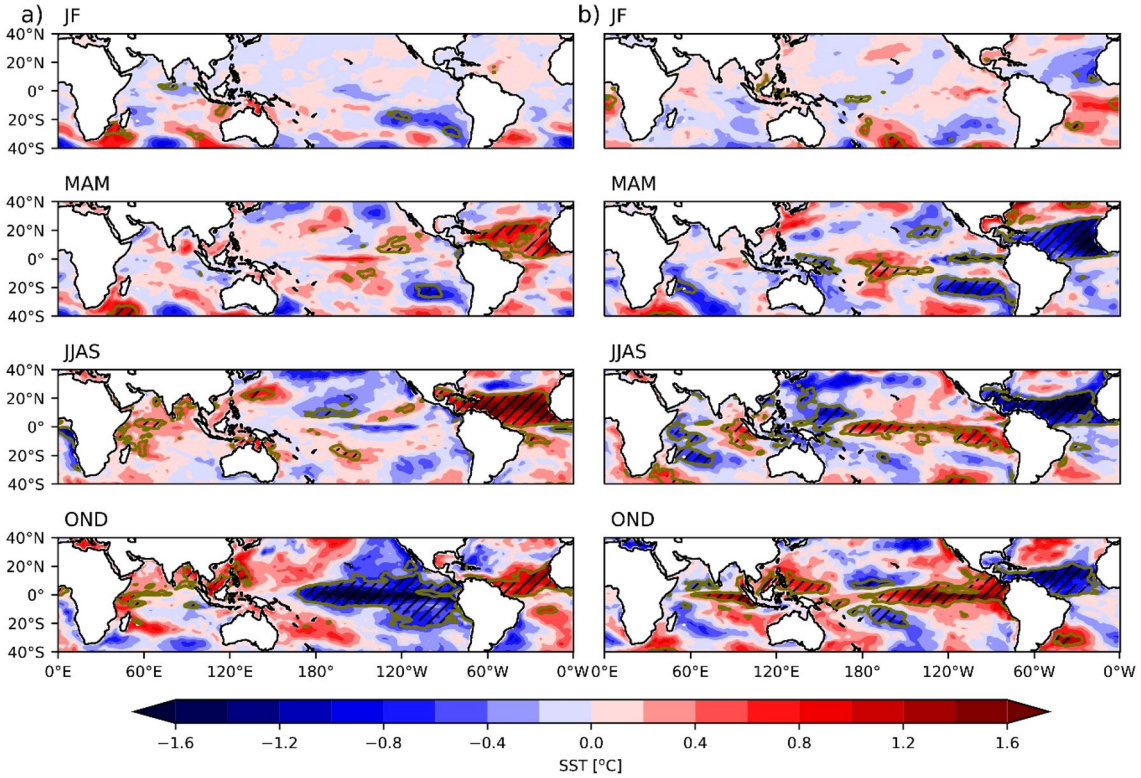

Fig. 9 Seasonal evolution (from January February, JF, to October to November, OND) in ensemble mean differences between the sensitivity and Pi-Control simulations for SST. **a** warmNTA_ElNinoIC_EXP minus ElNinoIC_PiCNTL and **b** coldNTA_LaNinaIC_EXP minus LaNinaIC_PiCNTL. See the detailed description at Sect. 2, for the computation of the ensemble mean differences between the sensitivity and Pi-Control simulations. Black hatches (olive contour), respectively, indicate the differences attaining 95% (90%) significance confidence level according to a two-tailed Student's *t*-test

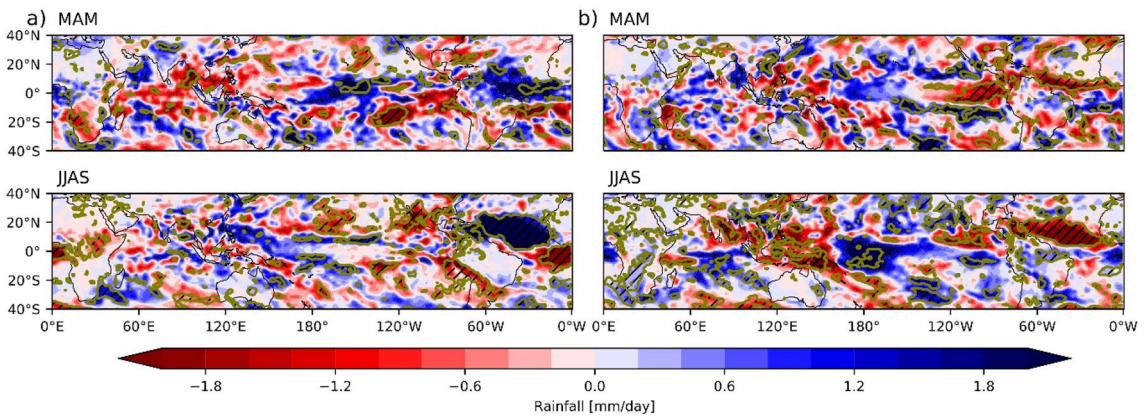

Fig. 10 Same as Fig. 9 but for the rainfall differences in MAM and JJAS seasons

For the coldNTA_LaNinaIC_EXP (again relative to Pi-Control), the ISMR response is negative over the Indian and surrounding oceanic regions, which coincides with the weakened low-level westerlies, thus reducing the moisture transport (from Arabian Sea) to the Indian landmass during JJAS (Figs. 10b, 11b). For the warmNTA_ElNinoIC_EXP, there is only insignificant rainfall response over India (Fig. 10a) with almost no changes in the low-level ISM circulation (Fig. 11a), and so the overall ISM response is quite weak. This is probably due to the fact that the Pacific SST response assumes feeble magnitudes (with weak cooling) during JJAS period (Fig. 9a) and hence not completely transitioned into La Niña state in the warmNTA_ElNinoIC_EXP relative to Pi-Control, while the El Niño develops faster and

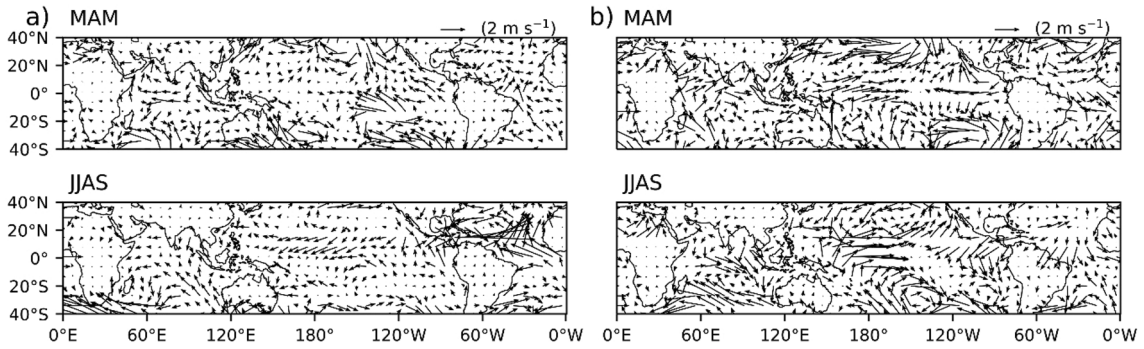

Fig. 11 Same as Fig. 10, but for the surface wind (ms^{-1})

significantly during JJAS in the coldNTA_LaNinaIC_EXP compared to Pi-Control. Cold equatorial Pacific SST differences between warmNTA_ElNinoIC_EXP and Pi-Control, emerge only two seasons later (i.e., OND). So, this late response is unable to significantly change the ENSO–ISM teleconnection during the boreal summer in warmNTA_ElNinoIC_EXP1 compared to Pi-Control. This illustrates the nonlinearity of the system and is also consistent with the observations in which cold NTA SSTs are a better precursor of ENSO changes than warm NTA SSTs (see Fig. 2).

In a nutshell, the sensitivity experiments confirm both the strong two-way interactions between NTA SSTs and the ENSO–ISM system, and the asymmetric features of these teleconnections in which the cold NTA SST perturbations are more influential than warm NTA SST one.

5 Discussion and summary

Recently, there is a growing recognition for the role of NTA SST anomalies as a key-driver of ENSO biennial variability due to its capacitor effect (Ham et al. 2013a, b; Wang et al. 2017). The NTA SSTs are also emerging as an important driver of the whole ENSO–ISM system, while AZM shows a very limited influence on ISMR variability during the recent decades (e.g., Ding et al. 2012). So, this study made an attempt to gain deeper insights on the teleconnection pathways linking NTA to ISMR as mediated by ENSO (i.e., NTA–ENSO–ISM relationship) using observations and a Pi-Control coupled simulation. To the best of our knowledge, there are only a few studies in this direction (Rong et al. 2010; Roy 2018; Vittal et al. 2020; Yang and Huang 2021; Terray et al. 2023).

We firstly showed that in both observation and IITM-ESM coupled model, the dominant mode of SST variability over NTA region exemplifies during MAM and is characterized by a basin-wide cold or warm SST anomaly. Secondly, most of the NTA events during boreal spring are initiated by previous ENSO conditions which illustrates the pronounced biennial nature of the ENSO-NTA system consistent with recent studies (e.g., Wang et al. 2017; Jiang and Li 2019; Park and Li 2019; Terray et al 2023). However, the relationship of NTA SST anomalies to the previous ENSO state is significantly exaggerated in IITM-ESM compared to the observations, thus eventually missing out the observed nonlinear characteristics. Such biases are found in many coupled models (Terray et al. 2023). The Pi-Control also misses the observed asymmetry in the role of NTA SSTs. In observations, the cold NTA SSTs seem a more significant precursor of the future evolution of the ENSO–ISM system than the warm ones (Roy 2018), while cold and warm NTA SSTs are equally important precursors in Pi-Control. Moreover, both the extratropical and tropical El Niño forcings dominate the warmNTA_LaNina and coldNTA_ElNino composites, and the role of NAO in triggering NTA SST anomalies is subsequently very limited in the Pi-Control, which is again in sharp contrast with the observations.

Due to the pairwise interactions between the three components of this NTA–ENSO–ISM system (i.e., tropical Pacific, Atlantic and Indian oceans; Cai et al. 2019; Terray et al. 2021, 2023), it is difficult to delineate the causes and effects underlying the NTA–ENSO–ISM relationship using these simple diagnostics. Furthermore, as the Pi-control is also unable to simulate the observed asymmetries as detailed above, it prompted us to conduct dedicated coupled sensitivity experiments focussing specifically on the nonlinearity of NTA SSTs in the ENSO–ISM system.

The sensitivity experiments consist of ensembles of short 1-year integrations carried out with the IITM-ESM model. Four 1-year long simulations are done starting from strong El Niño ICs (i.e., from January ICs) in the Pi-control and by imposing additional warm SST anomalies over NTA region (i.e., warmNTA_ElNinoIC_EXP). Similarly, four 1-year simulations using strong La Niña ICs are also done by imposing cold NTA SST anomalies (i.e., coldNTA_LaNinaIC_EXP). Thus, the sensitivity experiments are designed to assess the specific role of NTA SST anomalies in the

ENSO transitions and, subsequently, in the ENSO–ISM relationship.

First of all, the sensitivity experiments generally support the aforementioned remote teleconnections from NTA to ENSO conditions, thus illustrating the operational efficiency of the NTA capacitor effect, as the ENSO events are stronger during boreal winter (OND) in these short simulations. More importantly, these experiments also show nonlinear responses with respect to the polarity of the imposed NTA SST perturbations. In the warmNTA_ElNinoIC_EXP experiments, the Pacific SST response during JJAS period shows weak cooling (Fig. 9a) relative to the Pi-Control, with the complete transitioning of El Niño to La Niña state happening only two seasons later (i.e., OND). In contrast, in the coldNTA_LaNinaIC_EXP (compared to the Pi-Control, see Fig. 9b), there is a much faster transition from La Niña to El Niño state and El Niño conditions develop significantly as soon as in JJAS. The atmospheric response (i.e., suppressed rainfall and easterly low-level wind anomalies) over the northeastern Pacific during MAM holds a key role for this faster transition from La Niña to El Niño in the coldNTA_LaNinaIC_EXP (see Figs. 10b, 11b) thus exemplifying the role of off-equatorial Rossby wave response to the decreased rainfall over NTA region (Ham et al. 2013a). Another innovation comes from the modulation of the ENSO–ISM relationship in these experiments, as the cold NTA SST perturbations are associated with much drier conditions over India and a weaker ISM circulation, while the ISM response to warm NTA SST perturbations is mostly insignificant. This confirms the nonlinearity of the NTA–ENSO–ISM system, in which cold NTA SSTs are more influential than warm NTA SSTs, as seen in observations. This further adds new perspectives on the predictability of the whole ENSO–ISM system.

The identified non-linearities in the NTA–ENSO–ISM system are not highlighted in earlier studies to the best of our knowledge and, based on our results, we infer that it may be probably due to the unexplored role of NAOs, but also to deficiencies in IITM-ESM model in simulating the obseved ENSO skewness, which is a common problem in coupled models (e.g., Terray et al. 2021). But this needs further confirmation and hence warrants a more careful investigation. A natural extension of this study is also to conduct experiments starting from neutral ICs (instead using ENSO ICs), which may confirm that the NAO is important on its own in modulating NTA SSTs and the ENSO–ISM relationship. We also envisage to conduct additional experiments starting from ENSO ICs, but with reversed NTA SST polarity, for further understanding of the non-linearity of the NTA–ENSO–ISM system.

The specific role of the coupled model bias (particularly over the tropical Atlantic) needs also to be explored as this bias can also mute the response of the NTA–ENSO–ISM system in other coupled models (Kajtar et al. 2018; McGregor et al. 2018; Terray et al. 2023). In this context, one may wonder if the tropical Atlantic biases also play a role in the failure of the IITM-ESM coupled model to reproduce the nonlinearity of the NTA–ENSO–ISM system. For example, the spatio-temporal evolution in anomalous rainfall in the Pi-Control clearly shows the absence of observed dipole structure in rainfall anomalies over NTA region, though the NTA SST anomalies in both the composites exactly resemble the observed patterns. Interestingly, this erroneous rainfall response over the NTA region is partially rectified in the sensitivity experiments. This improved rainfall response is probably due to the rectification of coupled model bias, thanks to the imposed NTA SST forcing in the sensitivity experiments. However, the specific role of the model biases in our results deserves more detailed investigations and a lot of modelling efforts, which are outside the scope of our present study.

Finally, the NTA experiences a prominent (significant at 95% confidence level based on Mann–Kendall test, see Fig. S5) long-term linear warming in both annual (at a rate of 0.55 °C/decade) and boreal spring periods (at a rate of 0.22 °C/decade) from 1979 to 2017, which is much higher than in other tropical regions, especially in the eastern tropical Pacific. This may strengthen the local ocean–atmosphere coupling. As the climate variability over NTA region is also found to be intensifying under future warming scenario (Yang et al. 2021) and is modulating the ISM-ENSO teleconnection non-linearly following our results, a better understanding of the NTA–ENSO–ISM teleconnections in a warming climate is an issue of great significance for anticipating the effects of global warming in the ISM region (Douville et al. 2021). Furthermore, in the context of an increased interannual variability of ISMR in the coming decades (Katzenberger et al. 2021), more careful future projection studies on the changes in NTA–ENSO–ISM teleconnections are needed so as to mitigate the disastrous human effects of ISMR extremes at seasonal and longer time scales.

Supplementary Information The online version contains supplementary material available at https://doi.org/10.1007/s00382-023-06817-4.

Acknowledgements We sincerely thank Dr. R. Krishnan, Director, Indian Institute of Tropical Meteorology (IITM, India) and Dr. J. Sanjay, executive Director, Centre for Climate Change Research (CCCR at IITM) for all the support during the research study. Sooraj K P, Swapna P, Ajinkya M. Aswale and Sandeep N S are funded by the CCCR and IITM, which are fully funded by the Ministry of Earth Sciences, Government of India. Pascal Terray is funded by Institut de Recherche pour le Développement (IRD, France). We also thank IITM-ESM group for making the coupled model available for performing various simulations using the HPC resources at IITM.

Author contributions KPS, PS and PT contributed to writing the manuscript. AMA plotted the figures and analysed the results, and NSS conducted the coupled model simulations.

Funding The authors have no funding reference to declare.

Data availability Enquiries about data availability should be directed to the authors.

Declarations

Conflict of interest The authors have not disclosed any competing interests.

References

Adler RF, Sapiano MRP, Huffman GJ et al (2018) The Global Precipitation Climatology Project (GPCP) monthly analysis (new version 2.3) and a review of 2017 global precipitation. Atmosphere (basel) 9:138

Alexander MA, Bladé I, Newman M et al (2002) The atmospheric bridge: the influence of ENSO teleconnections on air–sea interaction over the global oceans. J Clim 15:2205–2231

Alexander MA, Vimont DJ, Chang P, Scott JD (2010) The impact of extratropical atmospheric variability on ENSO: testing the seasonal footprinting mechanism using coupled model experiments. J Clim 23:2885–2901

Amaya DJ, DeFlorio MJ, Miller AJ, Xie S-P (2017) WES feedback and the Atlantic meridional mode: observations and CMIP5 comparisons. Clim Dyn 49:1665–1679

Cabos W, de la Vara A, Koseki S (2019) Tropical atlantic variability: observations and modeling. Atmosphere (basel) 10:502

Cai W, Wu L, Lengaigne M et al (2019) Pantropical climate interactions. Science (1979) 363:6430. https://doi.org/10.1126/science.aav4236

Chakraborty A, Singhai P (2021) Asymmetric response of the Indian summer monsoon to positive and negative phases of major tropical climate patterns. Sci Rep 11:1–13

Cherchi A, Terray P, Ratna SB et al (2021) Indian ocean dipole influence on indian summer monsoon and enso: a review. Indian summer monsoon variability. Elsevier, Amsterdam, pp 157–182

Chiang JCH, Vimont DJ (2004) Analogous Pacific and Atlantic meridional modes of tropical atmosphere–ocean variability. J Clim 17:4143–4158

Chowdary J, Parekh A, Gnanaseelan C (2021) Indian summer monsoon variability teleconnections and beyond, Chap 8. Elsevier, Amsterdam, pp 157–182. ISBN: 978-0-12-822402-1. https://doi.org/10.1016/B978-0-12-822402-1.00011-9

Crétat J, Terray P, Masson S et al (2017) Indian Ocean and Indian summer monsoon: relationships without ENSO in ocean–atmosphere coupled simulations. Clim Dyn 49:1429–1448

Czaja A, van der Vaart P, Marshall J (2002) A diagnostic study of the role of remote forcing in tropical Atlantic variability. J Clim 15:3280–3290

Ding H, Keenlyside NS, Latif M (2012) Impact of the equatorial atlantic on the El Niño Southern Oscillation. Clim Dyn 38:1965–1972. https://doi.org/10.1007/s00382-011-1097-y

Douville H, Raghavan K, Renwick J et al (2021) Water cycle changes, Chap 8. Intergovernmental panel for climate change (IPCC), Working group 1 (WG1), Sixth assessment report (AR6)

Ek MB, Mitchell KE, Lin Y et al (2003) Implementation of Noah land surface model advances in the National Centers for Environmental Prediction operational mesoscale Eta model. J Geophys Res Atmos 108:D22

Eyring V, Bony S, Meehl GA et al (2016) Overview of the Coupled Model Intercomparison Project Phase 6 (CMIP6) experimental design and organization. Geosci Model Dev 9:1937–1958

García-Serrano J, Cassou C, Douville H et al (2017) Revisiting the ENSO teleconnection to the tropical North Atlantic. J Clim 30:6945–6957

Gill AE (1980) Some simple solutions for heat-induced tropical circulation. Q J R Meteorol Soc 106:447–462

Gregory JM, Bouttes N, Griffies SM et al (2016) The Flux-Anomaly-Forced Model Intercomparison Project (FAFMIP) contribution to CMIP6: investigation of sea-level and ocean climate change in response to CO_2 forcing. Geosci Model Dev 9:3993–4017

Griffies SM (2009) Elements of MOM4p1, GFDL ocean group technical report 6. NOAA/Geophysical Fluid Dynamics Laboratory

Ham YG, Kug JS (2015) Role of North Tropical Atlantic SST on the ENSO simulated using CMIP3 and CMIP5 models. Clim Dyn 45:3103–3117. https://doi.org/10.1007/s00382-015-2527-z

Ham YG, Kug JS, Park JY (2013a) Two distinct roles of Atlantic SSTs in ENSO variability: North Tropical Atlantic SST and Atlantic Niño. Geophys Res Lett 40:4012–4017. https://doi.org/10.1002/grl.50729

Ham YG, Kug JS, Park JY, Jin FF (2013b) Sea surface temperature in the north tropical Atlantic as a trigger for El Niño/Southern Oscillation events. Nat Geosci 6:112–116. https://doi.org/10.1038/ngeo1686

Hersbach H, Bell B, Berrisford P et al (2020) The ERA5 global reanalysis. Q J R Meteorol Soc 146:1999–2049

Jiang L, Li T (2019) Relative roles of El Niño-induced extratropical and tropical forcing in generating Tropical North Atlantic (TNA) SST anomaly. Clim Dyn 53:3791–3804. https://doi.org/10.1007/s00382-019-04748-7

Jiang L, Li T (2021) Impacts of tropical North Atlantic and equatorial Atlantic SST Anomalies on ENSO. J Clim 34:5635–5655

Kajtar JB, Santoso A, McGregor S et al (2018) Model under-representation of decadal Pacific trade wind trends and its link to tropical Atlantic bias. Clim Dyn 50:1471–1484. https://doi.org/10.1007/s00382-017-3699-5

Katzenberger A, Schewe J, Pongratz J, Levermann A (2021) Robust increase of Indian monsoon rainfall and its variability under future warming in CMIP6 models. Earth Syst Dyn 12:367–386

Kosaka Y, Xie SP (2013) Recent global-warming hiatus tied to equatorial Pacific surface cooling. Nature. https://doi.org/10.1038/nature12534

Kucharski F, Bracco A, Yoo JH, Molteni F (2008) Atlantic forced component of the Indian monsoon interannual variability. Geophys Res Lett. https://doi.org/10.1029/2007GL033037

Kucharski F, Bracco A, Yoo JH et al (2009) A Gill-Matsuno-type mechanism explains the tropical Atlantic influence on African and Indian monsoon rainfall. Q J R Meteorol Soc 135:569–579. https://doi.org/10.1002/qj.406

Lindzen RS, Nigam S (1987) On the role of sea surface temperature gradients in forcing low-level winds and convergence in the tropics. J Atmos Sci 44:2418–2436

Masson-Delmotte V, Zhai P, Pirani A, Connors SL, Péan C, Berger S, Caud N, Chen Y, Goldfarb L, Gomis M et al (2021) Climate change 2021: the physical science basis. In: Contribution of working group I to the sixth assessment report of the Intergovernmental Panel on Climate Change. Cambridge University Press

McGregor S et al (2018) Model tropical Atlantic biases underpin diminished Pacific decadal variability. Nat Clim Change 8:493–498a

Moorthi S, Pan HP, Caplan P (2001) Changes to the 2001 NCEP operational MRF/AVN global analysis/forecast system," NWS technical procedures bulletin, vol 484, pp 1–14. http://www.nws.noaa.gov/om/tpb/484.htm

Nath R, Luo Y, Chen W, Cui X (2018) On the contribution of internal variability and external forcing factors to the cooling trend

over the humid subtropical Indo-Gangetic Plain in India. Sci Rep 8:1–11
North GR, Bell TL, Cahalan RF, Moeng FJ (1982) Sampling errors in the estimation of empirical orthogonal functions. Mon Weather Rev 110:699–706
Ogata T, Morioka Y, Behera S (2019) Mid-latitude source of the ENSO-spread in SINTEX-F ensemble predictions. Clim Dyn 52:2613–2630
Pai DS, Rajeevan M, Sreejith OP et al (2014) Development of a new high spatial resolution (0.25 × 0.25) long period (1901–2010) daily gridded rainfall data set over India and its comparison with existing data sets over the region. Mausam 65:1–18
Park JH, Li T (2019) Interdecadal modulation of El Niño–tropical North Atlantic teleconnection by the Atlantic multi-decadal oscillation. Clim Dyn 52:5345–5360. https://doi.org/10.1007/s00382-018-4452-4
Parthasarathy B, Munot AA, Kothawale DR (1994) All-India monthly and seasonal rainfall series: 1871–1993. Theor Appl Climatol 49:217–224
Pottapinjara V, Roxy MK, Girishkumar MS et al (2021) Simulation of interannual relationship between the Atlantic zonal mode and Indian summer monsoon in CFSv2. Clim Dyn 57:353–373
Prodhomme C, Terray P, Masson S et al (2014) Impacts of Indian Ocean SST biases on the Indian Monsoon: as simulated in a global coupled model. Clim Dyn 42:271–290
Rayner NAA, Parker DE, Horton EB et al (2003) Global analyses of sea surface temperature, sea ice, and night marine air temperature since the late nineteenth century. J Geophys Res Atmos 108:D14
Ren H-C, Zuo J, Li W (2021) The impact of tropical Atlantic SST variability on the tropical atmosphere during boreal summer. J Clim 34:6705–6723
Rong X, Zhang R, Li T (2010) Impacts of Atlantic sea surface temperature anomalies on Indo-East Asian summer monsoon–ENSO relationship. Chin Sci Bull 55:2458–2468
Roy I (2018) Addressing on abrupt global warming, warming trend slowdown and related features in recent decades. Front Earth Sci 6:136. https://doi.org/10.3389/feart.2018.00136
Sabeerali CT, Ajayamohan RS, Bangalath HK, Chen N (2019) Atlantic zonal mode: an emerging source of Indian Summer Monsoon variability in a warming world. Geophys Res Lett 46:4460–4467. https://doi.org/10.1029/2019GL082379
Sabeerali CT, Ajayamohan RS, Praveen V (2022) Atlantic zonal mode-monsoon teleconnection in a warming scenario. Clim Dyn 58:1829–1843. https://doi.org/10.1007/s00382-021-05996-2
Sperber KR, Annamalai H, Kang I-S et al (2013) The Asian summer monsoon: an intercomparison of CMIP5 vs. CMIP3 simulations of the late 20th century. Clim Dyn 41:2711–2744
Storch HV, Zwiers FW (2002) Statistical analysis in climate research. Cambridge University Press, UK, p 494
Swapna P, Krishnan R, Sandeep N et al (2018) Long-term climate simulations using the IITM Earth System Model (IITM-ESMv2) with focus on the South Asian Monsoon. J Adv Model Earth Syst 10:1127–1149
Terray P, Masson S, Prodhomme C et al (2016) Impacts of Indian and Atlantic oceans on ENSO in a comprehensive modeling framework. Clim Dyn 46:2507–2533
Terray P, Sooraj KP, Masson S et al (2018) Towards a realistic simulation of boreal summer tropical rainfall climatology in state-of-the-art coupled models: role of the background snow-free land albedo. Clim Dyn 50:3413–3439
Terray P, Sooraj KP, Masson S, Prodhomme C (2021) Anatomy of the Indian Summer Monsoon and ENSO relationships in state-of-the-art CGCMs: role of the tropical Indian Ocean. Clim Dyn 56:329–356
Terray P, Joseph L, Sooraj KP (2023) Anatomy of the Indian summer monsoon and ENSO relationship in a state-of-the-art CGCM: role of the tropical Atlantic Ocean. Clim Dyn. https://doi.org/10.1007/s00382-022-06397-9
Trenberth KE, Branstator GW, Karoly D et al (1998) Progress during TOGA in understanding and modeling global teleconnections associated with tropical sea surface temperatures. J Geophys Res Oceans 103:14291–14324
Vimont DJ, Wallace JM, Battisti DS (2003) The seasonal footprinting mechanism in the Pacific: implications for ENSO. J Clim 16:2668–2675
Vittal H, Villarini G, Zhang W (2020) Early prediction of the Indian summer monsoon rainfall by the Atlantic Meridional Mode. Clim Dyn 54:2337–2346. https://doi.org/10.1007/s00382-019-05117-0
Wallace JM, Gutzler DS (1981) Teleconnections in the geopotential height field during the Northern Hemisphere winter. Mon Weather Rev 109:784–812
Wang C, Kucharski F, Barimalala R, Bracco A (2009) Teleconnections of the tropical Atlantic to the tropical Indian and Pacific Oceans: a review of recent findings. Meteorol Z 18:445–454. https://doi.org/10.1127/0941-2948/2009/0394
Wang L, Yu JY, Paek H (2017) Enhanced biennial variability in the Pacific due to Atlantic capacitor effect. Nat Commun. https://doi.org/10.1038/ncomms14887
Webster PJ, Magana VO, Palmer TN et al (1998) Monsoons: processes, predictability, and the prospects for prediction. J Geophys Res Oceans 103:14451–14510
Xie S-P, Carton JA (2004) Tropical Atlantic variability: Patterns, mechanisms, and impacts. Earth's Clim Ocean-Atmos Interact Geophys Monogr 147:121–142
Yang Y, Xie SP, Wu L et al (2018) ENSO forced and local variability of North Tropical Atlantic SST: model simulations and biases. Clim Dyn 51:4511–4524. https://doi.org/10.1007/s00382-017-3679-9
Yang Y, Wu L, Guo Y et al (2021) Greenhouse warming intensifies north tropical Atlantic climate variability. Sci Adv 7:eabg9690
Zebiak SE (1993) Air–sea interaction in the equatorial Atlantic region. J Clim 6:1567–1586